

# Experimental and theoretical study of neutral $\text{Al}_m\text{C}_n$ and $\text{Al}_m\text{C}_n\text{H}_x$ clusters

Feng Dong,<sup>a</sup> Scott Heinbuch,<sup>b</sup> Yan Xie,<sup>a</sup> Jorge J. Rocca<sup>b</sup> and Elliot R. Bernstein<sup>\*a</sup>

Received 21st October 2009, Accepted 18th December 2009

First published as an Advance Article on the web 27th January 2010

DOI: 10.1039/b922026g

Neutral  $\text{Al}_m\text{C}_n$  and  $\text{Al}_m\text{C}_n\text{H}_x$  clusters are investigated both experimentally and theoretically for the first time. Single photon ionization through 193, 118, and 46.9 nm lasers is used to detect neutral cluster distributions through time of flight mass spectrometry (TOFMS).  $\text{Al}_m\text{C}_n$  clusters are generated through laser ablation of a mixture of Al and C powders pressed into a disk. An oscillation of the vertical ionization energies (VIEs) of  $\text{Al}_m\text{C}_n$  clusters is observed in the experiments. The VIEs of  $\text{Al}_m\text{C}_n$  clusters change as a function of the numbers of Al and C atoms in the clusters.  $\text{Al}_m\text{C}_n\text{H}_x$  clusters are generated through an Al ablation plasma-hydrocarbon reaction, an Al–C ablation plasma reacting with  $\text{H}_2$  gas, or through cold  $\text{Al}_m\text{C}_n$  clusters reacting with  $\text{H}_2$  gas in a fast flow reactor. The VIEs of  $\text{Al}_m\text{C}_n\text{H}_x$  clusters are observed to vary as a function of the number of H atoms in the clusters. Density functional theory and *ab initio* calculations are carried out to explore the structures, ionization energies, and electronic structures of the  $\text{Al}_m\text{C}_n$  and  $\text{Al}_m\text{C}_n\text{H}_x$  clusters. C=C bonds are favored for the lowest energy structures for  $\text{Al}_m\text{C}_n$  clusters. H atoms can be bonded to either Al or C atoms in forming  $\text{Al}_m\text{C}_n\text{H}_x$  clusters, with little difference in energy. Electron density plots of the highest occupied molecular orbitals (HOMOs) for closed shell species and the singly occupied molecular orbitals (SOMOs) for open shell species of  $\text{Al}_m\text{C}_n$  and  $\text{Al}_m\text{C}_n\text{H}_x$  clusters are presented and described to help understand the physical and chemical properties of the observed species. VIEs do not simply depend on open or closed shell valence electron configurations, but also depend on the electronic structure details of the clusters. The calculational results provide a good and consistent explanation for the experimental observations, and are in general agreement with them. All calculated clusters are found to have a number of low lying isomeric structures.

## Introduction

Metal carbide clusters have been extensively studied as a new class of materials for semiconductors, ceramics, hydrogen storage, and catalysis. For example, met-cars are found to be particularly stable structures.<sup>1–3</sup> In order to elucidate the growth mechanisms for these special structures, geometric structures of metal carbide clusters have been investigated through both experimental<sup>3–10</sup> and theoretical studies.<sup>11–13</sup> Tono *et al.*<sup>4</sup> studied divanadium ( $\text{V}_2\text{C}_n^-$ ) and dicobalt ( $\text{Co}_2\text{C}_n^-$ ) anions as representative of dimetallic carbides of the early and late 3d transition metals, respectively. They found that the geometric structures of  $\text{Co}_2\text{C}_n^-$  clusters exhibit a tendency for carbon atoms to aggregate and form a  $\text{C}_n$  substructure, while  $\text{V}_2\text{C}_n^-$  clusters form a vanadium carbide network with  $\text{VC}_2$  building blocks. The structures of  $\text{Mo}_n\text{C}_{4n}$  are described as planar clusters of two, three, or four molybdenum atoms surrounded by carbon dimers.<sup>8</sup> Wang's group observed new prominent peaks in the  $\text{Ti}_x\text{C}_y^-$  anion

mass spectra derived from laser vaporization experiments, suggesting that  $\text{C}_2$  dimers, cubic framework, and layered structures play essential roles in determining the structures and chemical bonding of titanium carbide clusters.<sup>14,15</sup> Recently, Duncan *et al.* studied metal carbide cluster cations ( $\text{MC}_n^+$ ,  $n = \text{Cu, Au}$ ), and found that copper favors the formation of carbides with an odd number of carbon atoms, while gold shows a marked decrease in ion intensity after clusters with 3, 6, 9, and 12 carbons.<sup>16</sup> The structures of metal carbide clusters are highly dependent on the valence electronic configurations of the metals.

Aluminium carbide clusters, considered as non-classical and non-stoichiometric structures,<sup>17–22</sup> are different from most metal carbide clusters with cubic frameworks and layered structures.<sup>7,12,13</sup> Wang and co-workers studied small negative ion  $\text{Al}_m\text{C}_n^-$  clusters by photoelectron spectroscopy and *ab initio* calculations. They reported that  $\text{Al}_4\text{C}^{18}$  and  $\text{Al}_5\text{C}^{21a}$  cluster ions have tetracoordinate planar structures, an  $\text{Al}_2\text{C}_2$  cluster has a quasilinear (acetylenic) structure,<sup>19a</sup> and an  $\text{Al}_3\text{C}_2$  cluster is formed by attaching a third aluminium on one side of  $\text{Al}_2\text{C}_2$ .<sup>19b</sup> They also reported the first experimental and theoretical study of a salt-stabilized tetracoordinate planar carbon (TPC) dianion,  $\text{Na}^+[\text{CaI}_4^{2-}]$ .<sup>20</sup> Recently, Naumkin<sup>22</sup> calculated the structures of small  $\text{Al}_2\text{C}_n$  clusters, and concluded that all systems beyond  $\text{Al}_2\text{C}_2$  are structurally

<sup>a</sup> Department of Chemistry, NSF ERC for Extreme Ultraviolet Science and Technology, Colorado State University, Fort Collins, CO 80523, USA. E-mail: erb@lamar.colostate.edu

<sup>b</sup> Department of Electrical and Computer Engineering, NSF ERC for Extreme Ultraviolet Science and Technology, Colorado State University, Fort Collins, CO 80523, USA

different from their stoichiometric hydrocarbon counterparts due to ionic bonding of Al atoms to carbon molecular centers.

To date, no report is found for the experimental study of neutral aluminium carbide clusters. The distribution, definitive structures, and formation mechanisms for neutral  $\text{Al}_m\text{C}_n$  clusters are still not well known.  $\text{Al}_m\text{C}_n\text{H}_x$  clusters can be a potential material for hydrogen storage as complex aluminium hydrides  $\text{M}_m\text{Al}_n\text{H}_x$  ( $\text{M} = \text{Li}, \text{Na}, \text{Mg}, \text{B}, \text{Ti}, \text{Zr}$ ),<sup>23</sup> however, no experimental or theoretical study has been carried out on  $\text{Al}_m\text{C}_n\text{H}_x$  clusters.

In the present work, neutral aluminium carbide clusters ( $\text{Al}_m\text{C}_n$ ) and aluminium carbon hydride clusters ( $\text{Al}_m\text{C}_n\text{H}_x$ ) are observed and systematically studied for the first time. The neutral  $\text{Al}_m\text{C}_n$  clusters are generated by laser ablation of mixed aluminium/carbon targets into a carrier gas of pure helium. The neutral  $\text{Al}_m\text{C}_n\text{H}_x$  clusters can be generated by three different paths, involving  $\text{Al}_m\text{C}_n$  clusters plus  $\text{H}_2$  and  $\text{Al}_m$  clusters plus hydrocarbon. Based on single photon ionization (SPI) of these clusters with three different laser sources (6.4 eV/photon, 10.5 eV/photon, and 26.5 eV/photon), we find that both  $\text{Al}_m\text{C}_n$  and  $\text{Al}_m\text{C}_n\text{H}_x$  clusters have alternating VIEs related to the details of their respective open shell or closed shell electronic structures.

The structures of  $\text{Al}_m\text{C}_n$  and  $\text{Al}_m\text{C}_n\text{H}_x$  clusters are investigated through a comparison of experimental observations (that is, VIE and composition) and quantum chemistry calculational results. The VIEs of neutral  $\text{Al}_m\text{C}_n$  and  $\text{Al}_m\text{C}_n\text{H}_x$  clusters are calculated at the MP2/6-311+G\* level, at fixed equilibrium nuclear positions for these neutral species: the calculational results are in a good agreement with the experimental observations. The predicted structures for the calculated  $\text{Al}_m\text{C}_n$  and  $\text{Al}_m\text{C}_n\text{H}_x$  clusters are shown to be reasonable because cluster VIEs are in excellent agreement with the experimental results. Structures with C=C bonds are found to be energetically favorable for small neutral  $\text{Al}_m\text{C}_n$  clusters. The structures of  $\text{Al}_m\text{C}_n$  clusters are quite different from most other metal carbide clusters; these latter species tend to form a cubic frame structure.<sup>7,12,13</sup> These structural differences between  $\text{Al}_m\text{C}_n$  and  $\text{M}_m\text{C}_n$  clusters support the observation that hydrogen containing  $\text{Al}_m\text{C}_n\text{H}_x$  clusters can be generated under hydrocarbon plasma synthesis conditions, but that  $\text{M}_m\text{C}_n\text{H}_x$  clusters cannot be generated for the transition metals. Therefore,  $\text{Al}_m\text{C}_n\text{H}_x$  clusters have a unique property that suggests them as a potential hydrogen storage material.

## Experimental and theoretical methods

The experimental studies of neutral  $\text{Al}_m\text{C}_n$  and  $\text{Al}_m\text{C}_n\text{H}_x$  clusters involve a time of flight mass spectrometer (TOFMS) coupled with SPI at 193, 118, and 46.9 nm. The experimental apparatus and laser sources have been described in previous publications from this laboratory,<sup>24</sup> and therefore only a general outline of the experimental scheme will be presented in this report. Briefly, the neutral aluminium carbide clusters are generated in a conventional laser ablation/expansion source through laser ablation (focused 532 nm laser, 10–20 mJ pulse<sup>-1</sup>) of a mixed Al/C target into a carrier gas of pure helium gas (99.9995%) at 80 psi. The target is made by

pressing a mixture of carbon and aluminium powders. To generate aluminium carbon hydride clusters, three methods are used: (1) a pure aluminium foil (99.7%, Aldrich) target is used for laser ablation and a mixture of 5% hydrocarbon ( $\text{CH}_4$ ,  $\text{C}_2\text{H}_4$ , or  $\text{C}_2\text{H}_6$ ) and helium is used for the expansion gas; (2) a mixed Al/C target is used for laser ablation, and pure hydrogen is used for expansion gas; and (3) neutral aluminium carbide clusters are generated by ablation of an Al/C target, and then reacted with pure hydrogen gas in a fast flow reactor (70 mm length, Ø 6 mm), which is coupled directly to the cluster formation channel (40 mm length, Ø 1.8 mm). The ions created in the ablation source and fast flow reactor are removed by an electric field before the neutral clusters enter the ionization region. The instantaneous reactant gas mixture pressure in the reactor cell is about 1 ~ 2 Torr in this set up. In order to distinguish different  $\text{Al}_m\text{C}_n\text{H}_x$  clusters with the same mass (isobars) in the mass spectra, methane-d<sub>4</sub> (99 atom% D, Aldrich) and methane-<sup>13</sup>C (99 atom% <sup>13</sup>C, Aldrich) are also used as reactants in the experiments.

The soft X-ray laser (26.5 eV photon energy)<sup>25</sup> emits pulses of about 1 ns duration with an energy/pulse of 10 µJ that is reduced to 3 ~ 5 µJ after the light transverses a z-fold mirror system, and is not tightly focused in the ionization region to avoid multiphoton ionization and a Coulomb space charge effect due to  $\text{He}^+$  ions produced by 26.5 eV ionization of He in the molecular beam. We have previously, on the basis of our studies of metal, and metal oxide, and van der Waals clusters, proved that fragmentation caused by the high photon energy of the soft X-ray laser can be neglected.<sup>24–26</sup>

118 nm laser light is generated by focusing the third harmonic (355 nm, ~30 mJ pulse<sup>-1</sup>) of a Nd:YAG laser in a tripling cell that contains about a 250 Torr argon/xenon (10/1) gas mixture. To separate the generated 118 nm laser beam from the 355 nm fundamental beam, a magnesium fluoride prism (apex angle = 6°) is inserted into the laser light path. In this case, one is quite sure that mass signals are generated by ionization purely through the VUV laser radiation at low power (~1 µJ pulse<sup>-1</sup>, pulse duration ~5 ns). In these experiments, the fluence of an unfocused 193 nm laser is set to about 80 µJ cm<sup>-2</sup> pulse<sup>-1</sup> to avoid mutiphoton ionization of neutral clusters.

All the calculations reported in the present work are performed with the Gaussian03 program package.<sup>27</sup> The various possible lowest energy structures for small neutral  $\text{Al}_m\text{C}_n$  clusters are calculated at the B3LYP/6-311+G\* level of theory.<sup>28,29</sup> These structures are almost unchanged when they are refined using MP2 theory with the same basis set.<sup>30</sup> In all instances of these calculations for small  $\text{Al}_m\text{C}_n$  and  $\text{Al}_m\text{C}_n\text{H}_x$  species, the lowest energy clusters have singlet or doublet electronic structures.

The ionization energies for  $\text{Al}_m\text{C}_n$  and  $\text{Al}_m\text{C}_n\text{H}_x$  clusters are calculated at both theory levels by the following subtraction: for example,  $\text{VIE}(\text{Al}_m\text{C}_n\text{H}_x) = E(\text{Al}_m\text{C}_n\text{H}_x^+) - E(\text{Al}_m\text{C}_n\text{H}_x)$ , at fixed equilibrium nuclear positions for the  $\text{Al}_m\text{C}_n\text{H}_x$  neutral species. The MP2/6-311+G\* values are in better agreement with our experimental results than are those calculated at the B3LYP/6-311+G\* level. The B3LYP/6-311+G\* and MP2/6-311+G\* calculational methods have been used by Wang and Boldyrev *et al.*<sup>18–20</sup> to calculate the structures of

aluminium carbide anion clusters. Spin restricted (RHF) and spin unrestricted (UHF) wave functions are used for all closed shell and open shell systems, respectively. The molecular orbitals (MOs) for  $\text{Al}_m\text{C}_n$  and  $\text{Al}_m\text{C}_n\text{H}_x$  clusters are calculated at the B3LYP/6-311+G\* level. Wave function spin contamination is not a serious problem for open shell species at the B3LYP theory level, because  $\langle S^2 \rangle$  ( $S(S + 1)$ ) values are uniform and deviate only slightly from the pure spin value 0.75. B3LYP wave functions have also been used to calculate MOs of  $\text{AlC}_n/\text{AlC}_n^-/\text{AlC}_n^+$  clusters by Largo<sup>31</sup> and Li *et al.*<sup>32</sup> We also calculate MOs of these clusters at the MP2/6-311+G\* level; however, serious spin contamination is found for some of the open shell clusters. We perform DFT calculations to explore the highest occupied molecular orbitals (HOMOs) for neutral  $\text{Al}_m\text{C}_n$  and  $\text{Al}_m\text{C}_n\text{H}_x$  clusters (lowest energy structures) at the B3LYP/6-311+G\* level of theory. For open shell cluster, the highest occupied orbital is a singly occupied molecular orbital (SOMO). For the latter case, spin density and canonical orbital plots give nearly identical pictures because of the very small DFT spin polarization. Such orbital plots generate a physically useful understanding of the electronic, physical, and chemical properties of these clusters.

## Experimental results

### $\text{Al}_m\text{C}_n$ clusters

Neutral  $\text{Al}_m\text{C}_n$  clusters are generated in the ablation/expansion source in our experiments through laser ablation of an Al/C target into pure helium expansion gas. Fig. 1(a) displays the distribution of neutral  $\text{Al}_m\text{C}_n$  clusters ionized by SPI employing 193 nm light. Several series of the  $\text{Al}_m\text{C}_n$  clusters are identified in the mass spectrum; for example,  $\text{Al}_3\text{C}_2$ ,  $\text{Al}_3\text{C}_4$ ,  $\text{Al}_3\text{C}_6$ ,  $\text{Al}_3\text{C}_8$ , and  $\text{Al}_3\text{C}_{10}$ ,  $\text{Al}_5\text{C}$ ,  $\text{Al}_5\text{C}_3$ , and  $\text{Al}_5\text{C}_5$ , and  $\text{Al}_7\text{C}_2$  and  $\text{Al}_7\text{C}_4$ . Under the same experimental conditions, using the 26.5 eV soft X-ray laser for ionization, many more aluminium carbide clusters, including  $\text{Al}_2\text{C}_{2-4}$ ,  $\text{Al}_3\text{C}_{2-5}$ ,  $\text{Al}_4\text{C}_{2-6}$ , and  $\text{Al}_5\text{C}_{2-5}$ , are detected as shown in Fig. 1(b). Since the intensity of the soft X-ray laser is much lower than that of the 193 nm laser, the signal intensities in the experiments with soft X-ray laser ionization are much weaker than those derived by the 193 nm laser ionization; however, the distribution of neutral  $\text{Al}_m\text{C}_n$  clusters can still be identified.

### $\text{Al}_m\text{C}_n\text{H}_x$ clusters

Three methods are used to generate the  $\text{Al}_m\text{C}_n\text{H}_x$  clusters in the experiments. For method (1), pure aluminium foil is used as the ablation target, and mixtures of a hydrocarbon ( $\text{CH}_4$ ,  $\text{C}_2\text{H}_4$  or  $\text{C}_2\text{H}_6$ ) and He are used as the expansion gas. As shown in Fig. 2, an abundance of aluminium carbon hydride clusters is observed in the mass spectrum by using a 193 nm laser for SPI. For example, mass numbers 69 ( $\text{Al}_2\text{CH}_3$ ), 79 ( $\text{Al}_2\text{C}_2\text{H}$ ), 85 ( $\text{Al}_2\text{C}_2\text{H}_7/\text{Al}_3\text{H}_4$ ), 93 ( $\text{Al}_2\text{C}_3\text{H}_3$ ), 105 ( $\text{Al}_2\text{C}_4\text{H}_3/\text{Al}_3\text{C}_2$ ), 119 ( $\text{Al}_3\text{C}_3\text{H}_2/\text{Al}_2\text{C}_5\text{H}_5$ ), 129 ( $\text{Al}_3\text{C}_4/\text{Al}_2\text{C}_6\text{H}_3$ ), 145 ( $\text{Al}_4\text{C}_3\text{H}/\text{Al}_3\text{C}_5\text{H}_4$ ), 161 ( $\text{Al}_4\text{C}_4\text{H}_5/\text{Al}_5\text{C}_2\text{H}_2$ ), 171 ( $\text{Al}_4\text{C}_5\text{H}_3/\text{Al}_5\text{C}_3$ ), 185 ( $\text{Al}_5\text{C}_4\text{H}_2/\text{Al}_4\text{C}_6\text{H}_5$ ) amu, etc. are detected. Similar distributions of  $\text{Al}_m\text{C}_n\text{H}_x$  clusters are observed in Fig. 3 if the clusters are generated by using method (2), in which a mixed Al/C target is used for ablation,

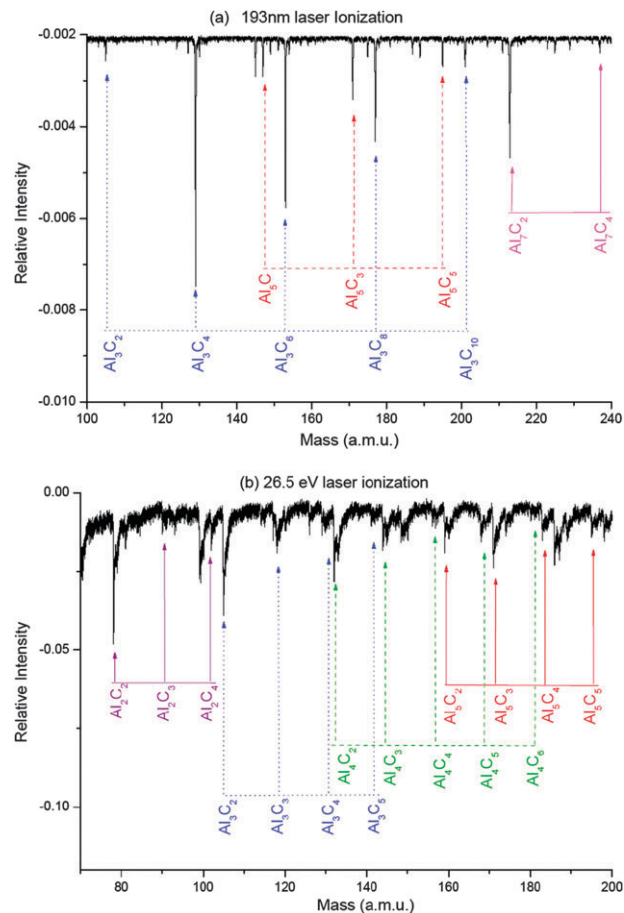
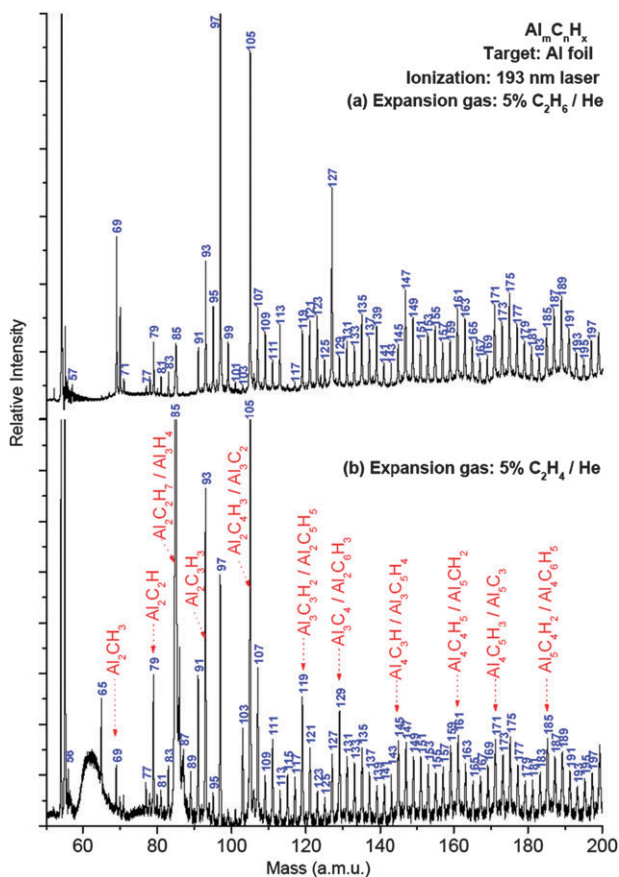


Fig. 1 Mass spectra of  $\text{Al}_m\text{C}_n$  clusters ionized by (a) a 193 nm (6.4 eV) UV laser and (b) a 46.9 nm (26.5 eV) soft X-ray laser. Clusters are generated by laser ablation of a mixed Al-C target into a pure He expansion gas at 80 psi backing pressure.

and pure  $\text{H}_2$  gas is used for expansion gas. For method (3), neutral  $\text{Al}_m\text{C}_n$  clusters are generated by ablation of a mixed Al/C target first, and then react with  $\text{H}_2$  molecules in a fast flow reactor after the expansion and cooling processes. As shown in Fig. 4, many new species are detected, such as  $\text{Al}_2\text{CH}_3$ ,  $\text{Al}_2\text{C}_3\text{H}_3$ ,  $\text{Al}_3\text{C}_3\text{H}_2$ ,  $\text{Al}_3\text{C}_4\text{H}_2$ ,  $\text{Al}_4\text{C}_3\text{H}$ ,  $\text{Al}_4\text{C}_4\text{H}$ , etc., which are generated from the reactions of  $\text{Al}_m\text{C}_n + \text{H}_2$  in the fast flow reactor. Note that all signals identified for  $\text{Al}_m\text{C}_n\text{H}_x$  clusters in the 193 nm SPI experiments are found for odd mass numbers (Fig. 2–4).  $\text{Al}_m\text{C}_n\text{H}_x$  clusters can also be detected by 118 nm laser SPI. As shown in Fig. 5, many signals are identified as  $\text{Al}_m\text{C}_n\text{H}_x$  clusters with both odd and even mass numbers; for example,  $\text{Al}_2\text{C}_2\text{H}_{1-12}$ ,  $\text{Al}_2\text{C}_3\text{H}_{1-12}$ ,  $\text{Al}_3\text{C}_2\text{H}_{1-12}$ ,  $\text{Al}_3\text{C}_3\text{H}_{1-12}$ , etc. This experimental observation must involve the ionization energies of the  $\text{Al}_m\text{C}_n\text{H}_x$  clusters. We investigate this issue through theoretical calculations of the structure, ionization energy, and highest occupied molecular orbital (HOMO/SOMO) energy of  $\text{Al}_m\text{C}_n\text{H}_x$  clusters. A comparison of the experimental results with calculated VIEs can be found in the Discussion section below.

In the studies of  $\text{Al}_m\text{C}_n$  and  $\text{Al}_m\text{C}_n\text{H}_x$  clusters, we take full advantage of the available three laser sources (193, 118, and 46.9 nm). Relatively high power can be provided by the 193 nm laser (unfocused,  $\sim 80 \mu\text{J}$ ), and a good signal to noise



**Fig. 2** Mass spectrum of  $\text{Al}_m\text{C}_n\text{H}_x$  clusters ionized by a 193 nm laser. Clusters are generated by laser ablation of pure Al foil into a mixture of (a) 5%  $\text{C}_2\text{H}_6/\text{He}$  and (b) 5%  $\text{C}_2\text{H}_4/\text{He}$  expansion gases at 80 psi backing pressure.

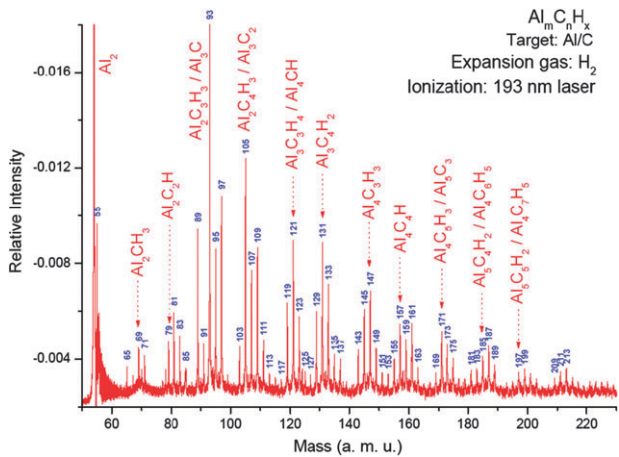


**Fig. 3** Mass spectrum of  $\text{Al}_m\text{C}_n\text{H}_x$  clusters ionized by a 193 nm laser. Clusters are generated by laser ablation of a mixed Al-C target into an  $\text{H}_2$  expansion gas at 80 psi backing pressure.

ratio can be obtained in the mass spectra; however, a single photon of 193 nm light cannot ionize all neutral clusters generated in the ablation/expansion source as shown in Fig. 1–4. A single photon (10.5 eV) from the 118 nm laser can ionize most of the neutral  $\text{Al}_m\text{C}_n$  and  $\text{Al}_m\text{C}_n\text{H}_x$  clusters with high resolution to distinguish one mass number difference

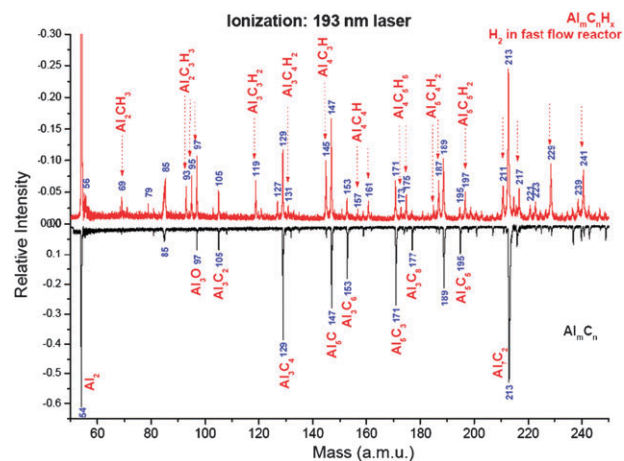


**Fig. 4**  $\text{Al}_m\text{C}_n\text{H}_x$  clusters generated through reactions of  $\text{Al}_m\text{C}_n$  clusters with  $\text{H}_2$  gas in a fast flow tube reactor. The  $\text{Al}_m\text{C}_n$  clusters are generated by ablation of a mixed Al-C target into an He expansion gas. Reactant gas  $\text{H}_2$  (15 psi backing pressure) is added to the fast flow reactor. New reaction products and remaining clusters are detected by 193 nm laser ionization.

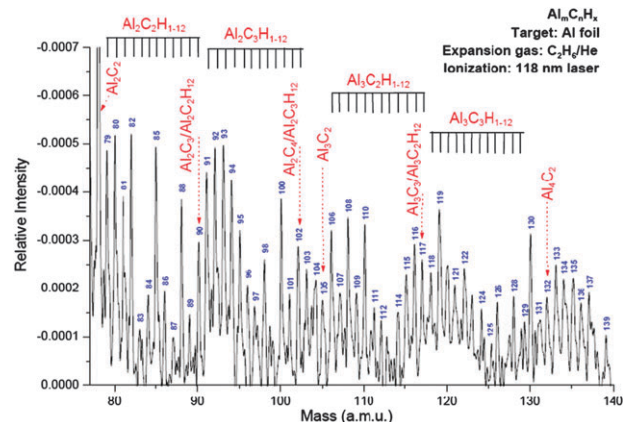


**Fig. 5** Mass spectrum of  $\text{Al}_m\text{C}_n\text{H}_x$  clusters ionized by a 118 nm laser. Clusters are generated by laser ablation of Al foil into a mixture of 5%  $\text{C}_2\text{H}_6/\text{He}$  expansion gas at 80 psi backing pressure. The signals are labeled by mass numbers. Some clusters  $\text{Al}_2\text{C}_2$  (78 amu),  $\text{Al}_2\text{C}_3/\text{Al}_2\text{C}_2\text{H}_{12}$  (90 amu),  $\text{Al}_3\text{C}_2$  (105 amu), and  $\text{Al}_3\text{C}_3/\text{Al}_3\text{C}_2\text{H}_{12}$  (117 amu) are labeled in the mass spectrum. The signals to higher mass of the labeled  $\text{Al}_m\text{C}_n$  clusters ( $\text{Al}_2\text{C}_2$ ,  $\text{Al}_2\text{C}_3$ ,  $\text{Al}_3\text{C}_2$ , and  $\text{Al}_3\text{C}_3$ ) are identified as  $\text{Al}_m\text{C}_n\text{H}_x$  cluster and are indicated at the top of the spectrum by  $\text{Al}_m\text{C}_n\text{H}_{1-12}$ .

at ca. 500 amu. The 118 nm, 10.5 eV laser is a good ionization source to detect  $\text{Al}_m\text{C}_n\text{H}_x$  clusters, as presented in Fig. 5; however, when a 118 nm laser is used to study  $\text{Al}_m\text{C}_n$  clusters, very weak signals are observed because the method of ablating the mixed Al/C target does not generate very many  $\text{Al}_m\text{C}_n$  clusters. The 46.9 nm soft X-ray laser is a unique ionization source that can ionize any neutral species generated in the molecular beam. Nonetheless, resolution of the mass spectrum obtained using 46.9 nm soft X-ray laser ionization is not as good as that observed with 118 nm laser ionization for the detection of  $\text{Al}_m\text{C}_n\text{H}_x$  clusters: the 46.9 nm soft X-ray laser is defocused in order to avoid multiphoton ionization and a space charge Coulomb effect due to  $\text{He}^+$  ions produced by

26.5 eV ionization of He (carrier gas) in the molecular beam. Additionally, spontaneous emission generated with the 46.9 nm laser degrades mass resolution for the detection of weak signals. Therefore, in the present experiments, we use 46.9 nm soft X-ray laser to detect  $\text{Al}_m\text{C}_n$  clusters (Fig. 1b), and use 118 nm laser to detect  $\text{Al}_m\text{C}_n\text{H}_x$  clusters in order to detect all neutral clusters generated in the cluster synthesis processes. Both ionization laser sources are essential components of these overall studies. Within this experimental regime, we have discovered the alternation of  $\text{Al}_m\text{C}_n$  and  $\text{Al}_m\text{C}_n\text{H}_x$  VIEs as presented above.

### Isotopic substitution experiments

The detected  $\text{Al}_m\text{C}_n\text{H}_x$  clusters can not all be uniquely distinguished and assigned in the mass spectra (Fig. 2, 3 and 4) due to mass degeneracy (isobars) for some of clusters; for example,  $\text{Al}_2\text{C}_3\text{H}_3$  and  $\text{Al}_3\text{C}$  have the same mass number (93 amu),  $\text{Al}_2\text{C}_4\text{H}_3$  and  $\text{Al}_3\text{C}_2$  have the same mass number (105 amu), etc. Many possible clusters of equal mass cannot be simply labeled in the mass spectra. In order to distinguish such clusters, isotopic  $\text{CD}_4/\text{He}$  and  $^{13}\text{CH}_4/\text{He}$  instead of  $^{12}\text{CH}_4/\text{He}$  mixtures are employed as the expansion gas to generate neutral  $\text{Al}_m\text{C}_n\text{H}_x$  clusters. As displayed in Fig. 6, the clusters  $\text{Al}_2\text{CH}_3$  (69 amu),  $\text{Al}_2\text{C}_2\text{H}$  (79 amu),  $\text{Al}_2\text{C}_3\text{H}_3$  (93 amu),  $\text{Al}_2\text{C}_4\text{H}_3/\text{Al}_3\text{C}_2$  (105 amu),  $\text{Al}_3\text{C}_3\text{H}_2$  (119 amu), etc. are distinguished and identified in the main distribution products of  $\text{Al}_m\text{C}_n\text{H}_x$  clusters. Note that the signal at mass number 105 amu (Fig. 6c) consists of two compounds ( $\text{Al}_2\text{C}_4\text{H}_3$  and  $\text{Al}_3\text{C}_2$ ). In the  $\text{CD}_4/\text{He}$  experiment (Fig. 6b), one identifies two peaks of 105 amu ( $\text{Al}_3\text{C}_2$ ) and 108 amu ( $\text{Al}_2\text{C}_4\text{D}_3$ ), which correspond to the peak of mass number 105 amu in the  $^{12}\text{CH}_4/\text{He}$  experiment (Fig. 6c). In the  $^{13}\text{CH}_4/\text{He}$  experiment, this peak is divided into the 107 ( $\text{Al}_3^{13}\text{C}_2$ ) and 109 ( $\text{Al}_2^{13}\text{C}_4\text{H}_3$ ) amu peaks as shown in Fig. 6a. Several series of  $\text{Al}_m\text{C}_n\text{H}_x$  clusters observed in Fig. 2–4 are identified as  $\text{Al}_2\text{CH}_{3,5}$ ,  $\text{Al}_2\text{C}_{2,3,5,7,9,11}$ ,  $\text{Al}_2\text{C}_3\text{H}_{1,3,5,7,9}$ ,  $\text{Al}_2\text{C}_4\text{H}_{3,5,7,9,11}$ ,  $\text{Al}_3\text{C}_2\text{H}_{2,4,6,8,10}$ ,  $\text{Al}_3\text{C}_3\text{H}_{2,4,6}$ ,  $\text{Al}_3\text{C}_4\text{H}_{2,4,6,8,10}$ ,  $\text{Al}_4\text{C}_3\text{H}_{1,3,5,7,9}$ ,  $\text{Al}_4\text{C}_4\text{H}_{1,3,5,7,9}$ ,  $\text{Al}_4\text{C}_5\text{H}_{1,3,5,7}$ ,  $\text{Al}_5\text{C}_4\text{H}_{2,4,6,8,10}$ , etc.

### Theoretical calculation results

#### Neutral $\text{Al}_m\text{C}_n$ clusters

**Structures.** The initial geometries of  $\text{Al}_m\text{C}_n$  cluster structural searches are based on generating C–C and Al–C bonds, since these bond strengths are much larger than Al–Al bond. We perform an exhaustive search for the initial geometries of  $\text{Al}_2\text{C}_2$ ,  $\text{Al}_2\text{C}_3$ ,  $\text{Al}_2\text{C}_4$ , and  $\text{Al}_3\text{C}_3$  clusters, and find that the formation of double and triple C–C bonds can stabilize  $\text{Al}_2\text{C}_n$  structures. The lowest energy isomers of  $\text{Al}_2\text{C}_5$  and  $\text{Al}_2\text{C}_6$  are found through connecting Al atoms with C atoms. The calculational results for  $\text{Al}_2\text{C}_2$ ,  $\text{Al}_2\text{C}_3$ , and  $\text{Al}_2\text{C}_4$ , and  $\text{Al}_2\text{C}_6$  are in good agreement with the reports of Naumkin<sup>22</sup> and Wang *et al.*<sup>19</sup> The present study is not aimed at an exhaustive search for all the various possible isomers of  $\text{Al}_m\text{C}_n$  clusters. The above cluster construction logic gives lowest energy structures of these small  $\text{Al}_m\text{C}_n$  clusters. The optimized lowest energy structures of clusters  $\text{Al}_2\text{C}_2$ ,  $\text{Al}_3\text{C}_2$ ,  $\text{Al}_4\text{C}_2$ ,  $\text{Al}_5\text{C}_2$ ,  $\text{Al}_6\text{C}_2$ ,  $\text{Al}_2\text{C}_4$  and  $\text{Al}_3\text{C}_3$  are presented in Fig. 7. The lowest

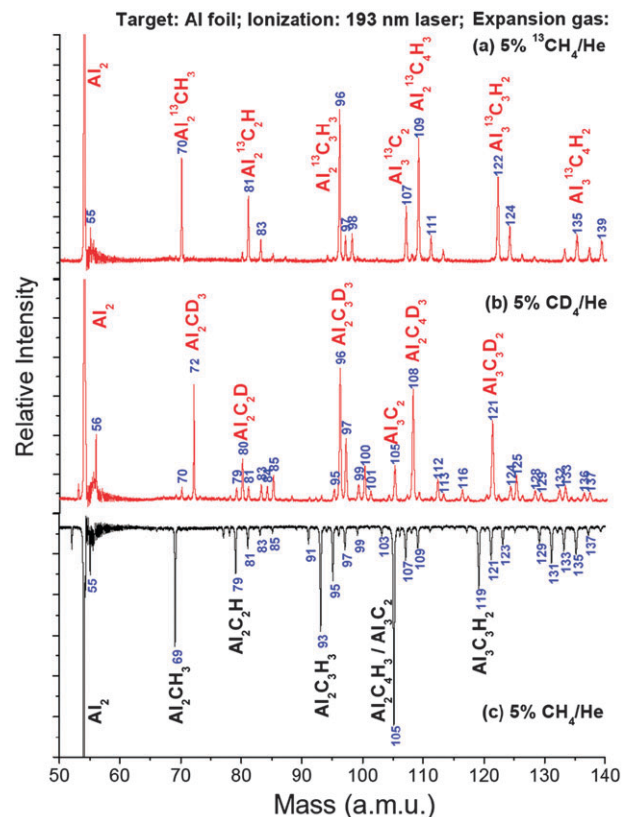


**Fig. 6** Mass spectra of  $\text{Al}_m\text{C}_n\text{H}_x$  clusters ionized by 193 nm laser. Clusters are generated by laser ablation of Al foil into a mixture of (a) 5%  $^{13}\text{CH}_4/\text{He}$ , (b) 5%  $\text{CD}_4/\text{He}$ , and (c) 5%  $\text{CH}_4/\text{He}$  expansion gas at 80 psi backing pressure.

energy isomer of  $\text{Al}_2\text{C}_2$  is a linear symmetric Al–C–C–Al structure like acetylene with two H atoms replaced by two Al atoms. The lowest energy structure for  $\text{Al}_3\text{C}_2$  is found to be a planar structure that can be described as adding one Al atom on one side of the  $\text{Al}_2\text{C}_2$  cluster. The lowest energy structure of the  $\text{Al}_4\text{C}_2$  cluster is also a planar structure, described as adding two Al atoms to the  $\text{Al}_2\text{C}_2$  cluster, one on each side of the Al–C–C–Al linear structure, bridging the C=C moiety. For the  $\text{Al}_5\text{C}_2$  cluster, the lowest energy structure has a nonplanar pentagonal shape, and for the  $\text{Al}_6\text{C}_2$  cluster, the lowest energy structure can be considered as adding two Al atoms on the top of a distorted  $\text{Al}_4\text{C}_2$  structure. The C–C bond lengths in these clusters are 1.26, 1.29, 1.34, 1.40, and 1.37 Å for  $\text{Al}_2\text{C}_2$ ,  $\text{Al}_3\text{C}_2$ ,  $\text{Al}_4\text{C}_2$ ,  $\text{Al}_5\text{C}_2$ , and  $\text{Al}_6\text{C}_2$  clusters, respectively. Additionally, the lowest energy structures for the  $\text{Al}_3\text{C}_3$  and  $\text{Al}_2\text{C}_4$  clusters can be formed from  $\text{Al}_3\text{C}_2$  and  $\text{Al}_2\text{C}_2$  by extending the C–C chain. All of the lowest energy structures of these neutral  $\text{Al}_m\text{C}_n$  clusters are found to be in singlet or doublet states for closed shell and open shell clusters, respectively. The lowest energy structures and ionization energies of neutral  $\text{Al}_2\text{C}_2$  (linear, VIE = 8.72 eV),  $\text{Al}_4\text{C}_2$  (planar, VIE = 8.22 eV),  $\text{Al}_6\text{C}_2$  (side-on, VIE = 7.86 eV) clusters are also calculated by Naumkin<sup>22</sup> at the MP2 and CCSD-T levels. The lowest energy structures calculated in ref. 22 are the same as presented herein, and the ionization energies of these clusters are also close to our results, as  $\text{Al}_2\text{C}_2$  (linear, VIE = 8.1 eV),  $\text{Al}_4\text{C}_2$  (flat, VIE = 7.6 eV), and  $\text{Al}_6\text{C}_2$  (side-on, VIE = 7.6 eV).

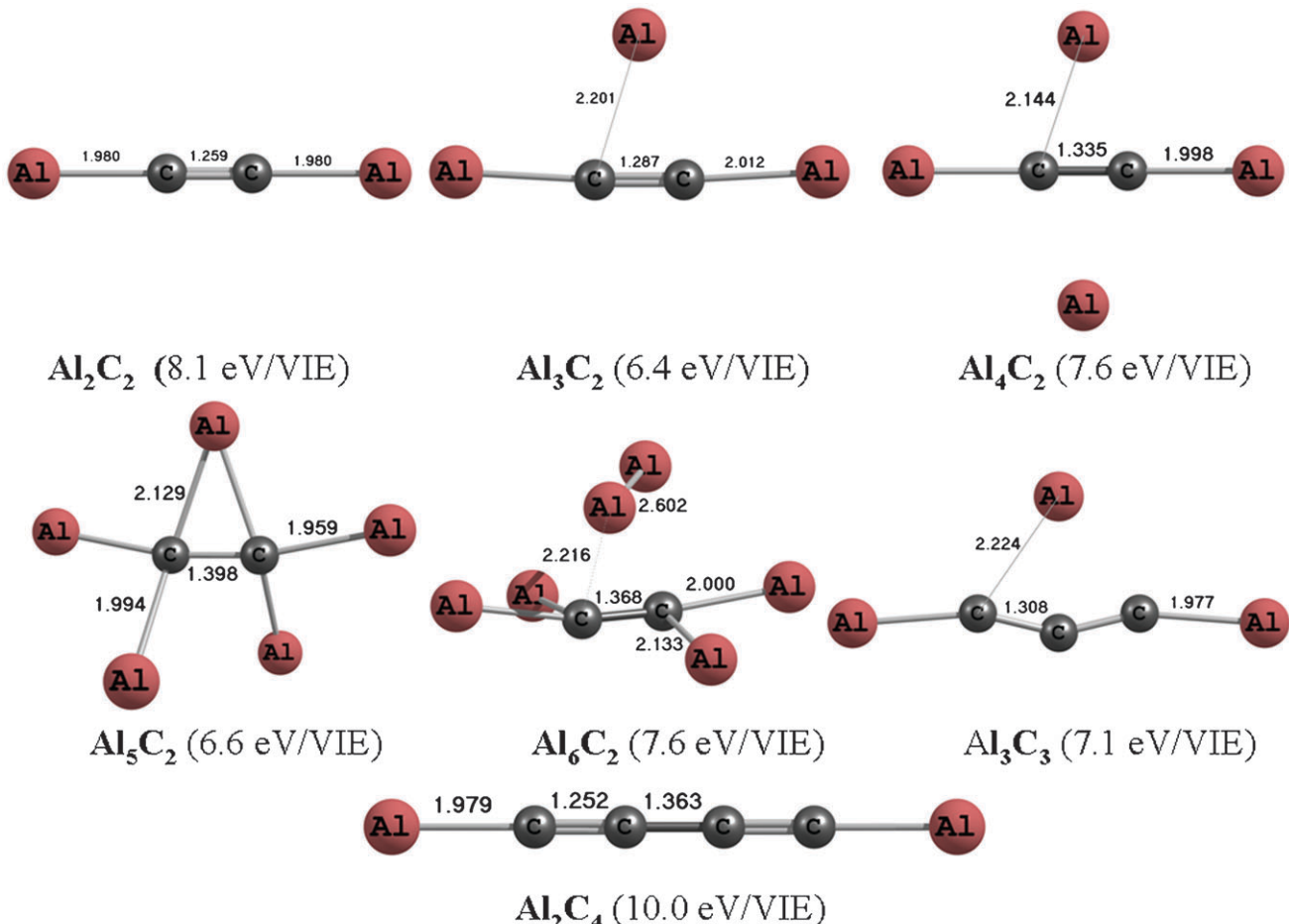


**Fig. 7** Lowest energy structures of small  $\text{Al}_m\text{C}_n$  cluster optimized at the MP2/6-311+G\* theory level. Values (in eV) in parentheses below each geometry are VIEs for the clusters calculated at the same theory level.

**VIEs.** VIEs for the lowest energy structures of  $\text{Al}_m\text{C}_n$  clusters are calculated at the MP2/6-311+G\* level of theory. As pointed out in Methods section the VIEs are calculated directly for the fixed, equilibrium, neutral ground state structure. These results are in qualitative agreement with VIEs calculated by Koopman's theorem and are consistent with the general notions of bonding and antibonding orbital relative energies. Based on such calculations, VIEs for  $\text{Al}_m\text{C}_2$  clusters are  $\text{Al}_2\text{C}_2$  (8.1 eV),  $\text{Al}_4\text{C}_2$  (7.6 eV),  $\text{Al}_6\text{C}_2$  (7.6 eV),  $\text{Al}_3\text{C}_2$  (6.4 eV), and  $\text{Al}_5\text{C}_2$  (6.6 eV), respectively. In Fig. 8, VIEs of neutral  $\text{Al}_m\text{C}_2$  clusters are plotted against the number of Al atoms in the clusters. Additionally, the VIEs for  $\text{Al}_3\text{C}_3$  and  $\text{Al}_2\text{C}_4$  cluster are calculated to be 7.1 and 10.0 eV, respectively.

**Molecular orbitals.** We also perform DFT calculations to explore the highest occupied molecular orbitals (HOMOs/SOMOs) for neutral  $\text{Al}_m\text{C}_n$  clusters (lowest energy structures) at the B3LYP/6-311+G\* level of theory. As shown in Fig. 9, the HOMO of the  $\text{Al}_2\text{C}_2$  cluster is primarily an out of phase combination of two non bonding Al orbitals (s and s/p atomic orbitals) with a C–C  $\sigma$  bonding orbital. This HOMO for  $\text{Al}_2\text{C}_2$  is mainly a  $\sigma$ -type orbital localized on the Al atoms. The SOMO of the  $\text{Al}_3\text{C}_2$  cluster is obviously a combination of a C–C antibonding  $\pi$  orbital and bonding C–Al and Al–Al

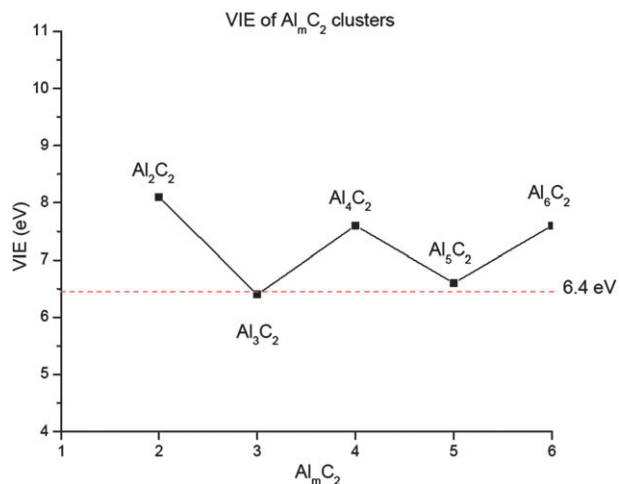


**Fig. 8** The VIEs of  $\text{Al}_m\text{C}_2$  clusters plotted against the number of Al atoms m in the clusters. (Calculated at the MP2/6-311+G\* theory level.)

orbitals. The HOMO of the  $\text{Al}_4\text{C}_2$  cluster can be characterized by a C–C  $\pi$  orbital with contributions from the non bonding orbitals of two bridging Al atoms (s and s/p atomic orbitals). For the  $\text{Al}_5\text{C}_2$  cluster, a C–C antibonding  $\pi$  orbital and a

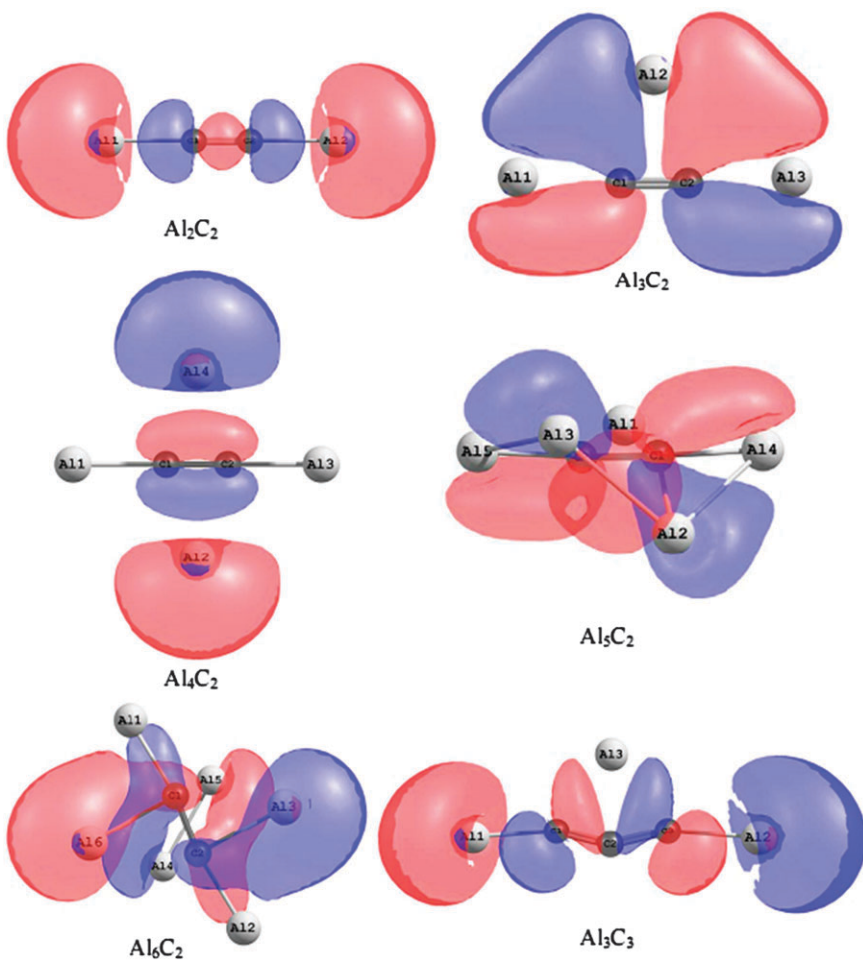


**Fig. 9** HOMOs/SOMOs for the lowest energy  $\text{Al}_m\text{C}_n$  structures calculated at the B3LYP/6-311 + G\* level.

bonding  $\sigma$  orbital of Al–Al contribute to the cluster's SOMO. The HOMO for the  $\text{Al}_6\text{C}_2$  cluster can be described as derived from  $\sigma$  bonding orbitals formed between Al and C atoms with a very slight contribution from a C–C antibonding  $\pi$  orbital. Additionally, the SOMO of the  $\text{Al}_3\text{C}_3$  cluster is composed of a C–C–C antibonding  $\pi$  orbital and the non bonding orbitals of two end Al atoms. Calculated spin densities for open shell  $\text{Al}_m\text{C}_n$  ( $\text{Al}_3\text{C}_2$ ,  $\text{Al}_5\text{C}_2$ ,  $\text{Al}_3\text{C}_3$ ) and  $\text{Al}_2\text{C}_2\text{H}_x$  ( $\text{Al}_2\text{C}_2\text{H}$ ,  $\text{Al}_2\text{C}_2\text{H}_3$ ) clusters can be characterized as antibonding  $\pi$  distributions that are similar to the SOMOs generated by DFT calculations. Thus, we follow the lead of Simons and coworkers<sup>17–21</sup> and plot canonical orbitals derived from the B3LYP/6-311 + G\* theory level for which the  $\langle S^2 \rangle < 0.77$  in all instances for open shell systems.

#### Neutral $\text{Al}_m\text{C}_n\text{H}_x$ clusters

**Structures.** In the present study, all the isomers of  $\text{Al}_2\text{C}_2$  are considered to form three dimensional  $\text{Al}_2\text{C}_2\text{H}_x$  conformations in order to find lowest energy structures. Bridging hydrogen structures are also considered for these initial structures. Fig. 10 shows the two lowest energy structures for various  $\text{Al}_2\text{C}_2\text{H}_x$  clusters, isomers (a) and (b). The lowest energy  $\text{Al}_2\text{C}_2\text{H}_x$  clusters are found to be in the lowest spin states (singlet states for closed shell and doublet states for open shell)

for each cluster at both the B3LYP and MP2 theory levels. The stable structures for these  $\text{Al}_2\text{C}_2\text{H}_x$  clusters are shown in Fig. 10 as optimized at the B3LYP/6-311 + G\* level of theory. All the lowest energy structures found at the B3LYP level are the same as those found for the MP2 level except for  $\text{Al}_2\text{C}_2\text{H}_4$ : the energy of isomer (a) is 0.05 eV higher than that of isomer (b) at the MP2 level (see Fig. 10). For clusters containing one H atom ( $\text{Al}_2\text{C}_2\text{H}$ ), the isomer  $\text{Al}_2\text{C}_2\text{H}_{\text{a}}$  is the lowest energy structure, in which the H atom bonds to a C atom and the  $\text{Al}_2\text{C}_2$  moiety is changed from linear to planar. If the H atom bonds to an Al atom to form isomer  $\text{Al}_2\text{C}_2\text{H}_{\text{b}}$ , the energy increases 0.07 eV relative to the lowest energy isomer  $\text{Al}_2\text{C}_2\text{H}_{\text{a}}$ . For clusters containing two H atoms ( $\text{Al}_2\text{C}_2\text{H}_2$ ), the lowest energy isomer is  $\text{Al}_2\text{C}_2\text{H}_{\text{a}}$  formed by adding two H atoms on one Al atom of the  $\text{Al}-\text{C}=\text{C}-\text{Al}$  cluster. The second lowest energy isomer is found to be  $\text{Al}_2\text{C}_2\text{H}_{\text{b}}$ , in which two H atoms are bonded to the two C atoms joined by a  $\text{C}=\text{C}$  bond. The isomer  $\text{Al}_2\text{C}_2\text{H}_{\text{b}}$  is 0.43 eV higher in energy than the isomer  $\text{Al}_2\text{C}_2\text{H}_{\text{a}}$ . For the lowest energy structure of  $\text{Al}_2\text{C}_2\text{H}_3$  (a), two H atoms bond to one Al atom and the other H atom bonds to a C atom of the  $\text{C}=\text{C}$  bond.  $\text{Al}_2\text{C}_2\text{H}_{\text{b}}$  is formed by connecting the three H atoms to two Al atoms. Their energy is slightly higher than that of  $\text{Al}_2\text{C}_2\text{H}_{\text{a}}$  by 0.05 eV. For the  $\text{Al}_2\text{C}_2\text{H}_4$  cluster, the lowest energy isomer structure  $\text{Al}_2\text{C}_2\text{H}_{\text{a}}$  can be formed by adding four H atoms to

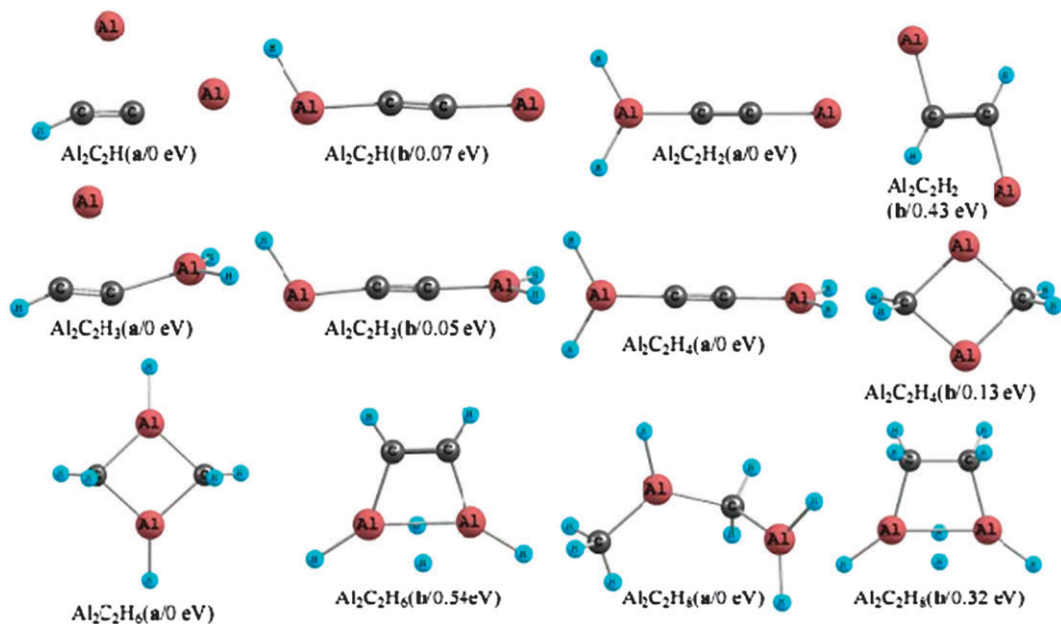


**Fig. 10** Optimized geometries for various  $\text{Al}_2\text{C}_2\text{H}_x$  cluster at the B3LYP/6-311+G\* theory level. The isomer (a) and (b) are two lowest energy structures. Values (in eV) in parentheses below each geometry are the isomer energies relative to lowest energy isomer a.

the Al atoms of the Al-C=C-Al cluster. An Al-C-Al-C four-membered ring structure is found as isomer  $\text{Al}_2\text{C}_2\text{H}_4\text{-b}$ , in which the four H atoms are connected to the two C atoms. The energy for isomer  $\text{Al}_2\text{C}_2\text{H}_4\text{-b}$  is 0.13 eV higher than that of isomer  $\text{Al}_2\text{C}_2\text{H}_4\text{-a}$ .

Some possible isomers for the clusters containing 6 and 8 H atoms are also investigated. The lowest energy isomer for  $\text{Al}_2\text{C}_2\text{H}_6$  cluster is an Al-C-Al-C four-membered ring structure like  $\text{Al}_2\text{C}_2\text{H}_6\text{-a}$ , and the second lowest energy structure is  $\text{Al}_2\text{C}_2\text{H}_6\text{-b}$ , a four-membered ring structure with a C=C double bond in which two H atoms are in a bridge position relative to the Al-Al moiety, and the other four H atoms bond with two Al and two C atoms. Isomers  $\text{Al}_2\text{C}_2\text{H}_6\text{-b}$

has higher energies than isomer  $\text{Al}_2\text{C}_2\text{H}_6\text{-a}$  by 0.54 eV. For the cluster  $\text{Al}_2\text{C}_2\text{H}_8$ , the lowest energy molecule is  $\text{Al}_2\text{C}_2\text{H}_8\text{-a}$ , a chain structure of C-Al-C-Al saturated by H atoms similar to an alkane structure. Additionally, a four-membered ring (Al-C-C-Al) structure ( $\text{Al}_2\text{C}_2\text{H}_8\text{-b}$ ) is also found. It has higher energy than  $\text{Al}_2\text{C}_2\text{H}_8\text{-a}$  by 0.32 eV.

**VIEs.** The lowest energy structures for the  $\text{Al}_2\text{C}_2\text{H}_{1-4}$  and  $\text{Al}_3\text{C}_2\text{H}_{1,2}$  clusters are refined at the MP2/6-311+G\* theory level, and VIEs for these clusters are calculated at the same level, as explained above. The VIEs for  $\text{Al}_2\text{C}_2$ ,  $\text{Al}_2\text{C}_2\text{H}$ ,  $\text{Al}_2\text{C}_2\text{H}_2$ ,  $\text{Al}_2\text{C}_2\text{H}_3$ , and  $\text{Al}_2\text{C}_2\text{H}_4$  clusters are 8.1, 6.3, 8.7, 7.0, and 10.3 eV, respectively. The VIEs of  $\text{Al}_2\text{C}_2\text{H}_x$  clusters are plotted against the number of H atoms in the clusters as shown in Fig. 11. Additionally, the VIEs of  $\text{Al}_3\text{C}_2\text{H}_1$  and  $\text{Al}_3\text{C}_2\text{H}_2$  clusters are calculated as 7.5 and 6.9 eV, respectively.

**Molecular orbitals.** The HOMOs/SOMOs for the  $\text{Al}_2\text{C}_2\text{H}_{1-4}$  and  $\text{Al}_3\text{C}_2\text{H}_{1,2}$  clusters calculated at the B3LYP/6-311+G\* level of theory are plotted in Fig. 12. SOMOs for the  $\text{Al}_2\text{C}_2\text{H}$  and  $\text{Al}_2\text{C}_2\text{H}_3$  clusters are primarily C=C antibonding  $\pi$  in character. The HOMO of the  $\text{Al}_2\text{C}_2\text{H}_2$  cluster is mainly composed of a non bonding orbital of an Al atom (atomic features s and sp orbitals). For the  $\text{Al}_2\text{C}_2\text{H}_4$  cluster, the HOMO is characterized by a bonding C=C  $\pi$  orbital. The HOMO for the  $\text{Al}_3\text{C}_2\text{H}_1$  cluster consists of a distorted anti-bonding  $\pi$  C=C orbital and Al and H atomic valence orbitals. And the SOMO of the  $\text{Al}_3\text{C}_2\text{H}_2$  cluster is primarily C=C antibonding  $\pi$  in character, similar to the SOMO of  $\text{Al}_3\text{C}_2$ .

## Discussion

### $\text{Al}_m\text{C}_n$ clusters

Neutral  $\text{Al}_m\text{C}_n$  clusters are generated through the ablation of a mixed Al-C target into pure He expansion gas. As shown in

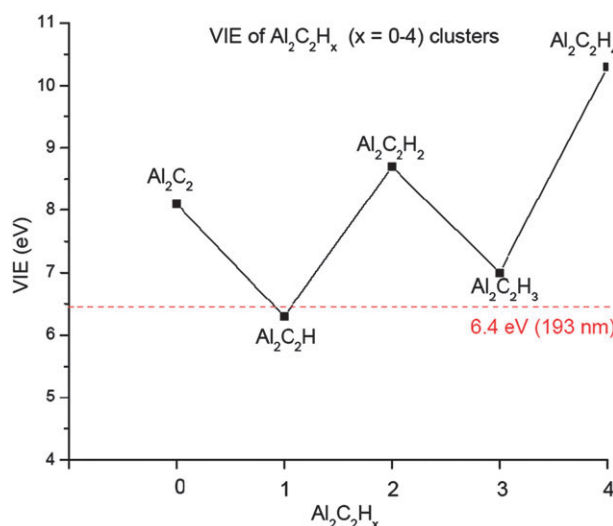


**Fig. 11** VIEs of  $\text{Al}_2\text{C}_2\text{H}_x$  clusters plotted against the number of H atoms x in the clusters. (Calculated at the MP2/6-311+G\* theory level.)

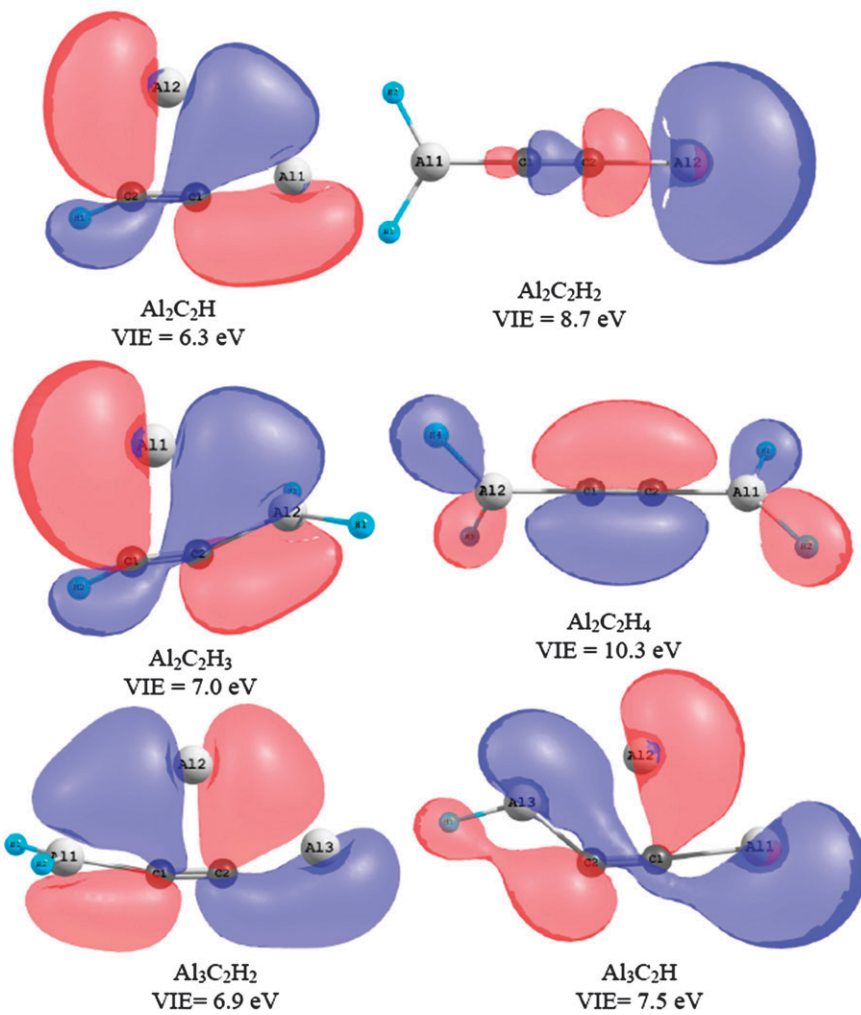


**Fig. 12** HOMOs/SOMOs for the lowest energy  $\text{Al}_2\text{C}_2\text{H}_{1-4}$  and  $\text{Al}_3\text{C}_2\text{H}_{1,2}$  cluster structures calculated at the B3LYP/6-311+G\* theory level. Values (in eV) in parentheses below each cluster are the VIEs for the clusters calculated at the MP2/6-311+G\* theory level.

Fig. 1a, several series of  $\text{Al}_m\text{C}_n$  clusters are detected by SPI at 193 nm:  $\text{Al}_3\text{C}_{2n}$  ( $n = 1-5$ ),  $\text{Al}_5\text{C}_{2n+1}$  ( $n = 0-2$ ), and  $\text{Al}_7\text{C}_{2n}$  ( $n = 1, 2$ ). These clusters should have lower ionization energies than 6.4 eV. Note that these signals identified for  $\text{Al}_m\text{C}_n$  clusters have odd mass numbers in the mass spectrum. Under the same experimental conditions, all  $\text{Al}_m\text{C}_n$  clusters are detected by SPI of the 26.5 eV soft X-ray laser (see Fig. 1b). One knows that the photon energy of the soft X-ray laser is high enough to ionize all neutral species. This experimental observation indicates that all aluminium carbide clusters  $\text{Al}_m\text{C}_n$  ( $m \leq 7, n \leq 10$ ) are generated in the experiment. We have previously, on the basis of our studies of metal and metal oxide clusters<sup>24</sup> and van der Waals clusters,<sup>33</sup> proved that fragmentation caused by the high photon energy of the soft X-ray laser can be neglected. Through comparison of the 193 nm and soft X-ray experimental results, we find that the following  $\text{Al}_m\text{C}_n$  clusters are not detected by 193 nm SPI due to their high ionization energies: (1)  $\text{Al}_m\text{C}_n$  clusters with an even number of aluminium atoms, such as  $\text{Al}_2\text{C}_n$ ,  $\text{Al}_4\text{C}_n$ ,  $\text{Al}_6\text{C}_n$  etc; (2) the  $\text{Al}_3$  family with odd numbers of C atoms ( $\text{Al}_3\text{C}_{2n+1}$ ); (3) the  $\text{Al}_5$  family with an even number of C atoms ( $\text{Al}_5\text{C}_{2n}$ ); and (4) the  $\text{Al}_7$  family with odd an number of C

atoms ( $\text{Al}_7\text{C}_{2n+1}$ ). Experimental observation indicates that the ionization energies of the  $\text{Al}_m\text{C}_n$  clusters systematically change with both the number of Al atoms and C atoms.

Theoretical calculations are performed to study the structures of  $\text{Al}_m\text{C}_n$  clusters. Based on the calculations, a C–C bond is formed for the lowest energy structures of  $\text{Al}_m\text{C}_2$  clusters, such as  $\text{Al}_2\text{C}_2$ ,  $\text{Al}_3\text{C}_2$ ,  $\text{Al}_4\text{C}_2$ ,  $\text{Al}_5\text{C}_2$ , and  $\text{Al}_6\text{C}_2$ , as shown in Fig. 7. The bond length for the C–C moiety for the lowest energy structure of  $\text{Al}_2\text{C}_2$  (1.26 Å) and  $\text{Al}_3\text{C}_2$  (1.29 Å) are longer than the triple bond of acetylene (1.22 Å), but shorter than the double bond of ethylene (1.34 Å). The C–C bond for the  $\text{Al}_4\text{C}_2$  (1.34 Å) clusters is close to that of a C=C hydrocarbon double bond, and slightly shorter than the C=C double bonds for  $\text{Al}_5\text{C}_2$  (1.40 Å) and  $\text{Al}_6\text{C}_2$  (1.37 Å) clusters. The C–C bond lengths in these clusters increase with the number of Al atoms with the exception of  $\text{Al}_6\text{C}_2$ . Additionally, C=C chains are also formed in the lowest energy structures of  $\text{Al}_3\text{C}_3$  and the  $\text{Al}_2\text{C}_4$  clusters, further indicating that structures with C=C bonds are energetically favorable for small neutral  $\text{Al}_m\text{C}_n$  clusters. The structures of aluminium carbide clusters are quite different from most other metal carbide clusters; these latter species tend to form cubic

frame structures due to relatively strong ionic bonds between the metal and carbon atoms.<sup>7,12,13</sup> The bond strengths of the metal–Carbon bonds apparently strongly influence and eventually decide the structures of metal carbides. The strength of Al–C bond is 3.51 eV,<sup>22</sup> much weaker than for transition metal–Carbon bonds, for example, Ti–C (4.5 eV) and V–C (4.9 eV).<sup>34</sup>

A significant even–odd alternation with respect to the number  $m$  of Al atom in a cluster is found for the VIEs of neutral  $\text{Al}_m\text{C}_n$  clusters, as plotted in Fig. 8. The calculational results are in very good agreement with the experimental observations. This agreement between calculated and observed VIEs, and especially the overall trend in VIEs, indicates that the calculated electronic and geometric structures of the clusters are believable, and further, that their calculated formation mechanisms and chemical reactivity can be realistically explored through a similar level of theory.

Aluminium and carbon atoms have 13 and 6 electrons, respectively. The valence electron configurations of neutral  $\text{Al}_m\text{C}_n$  clusters thus change from closed to open shell with even and odd numbers of Al atoms in the clusters. Ionization energies of  $\text{Al}_m\text{C}_n$  clusters change with valence electron configurations of the neutral clusters. This behavior can not be explained simply based on the general concept that closed shell clusters ( $\text{Al}_2\text{C}_2$ ,  $\text{Al}_4\text{C}_2$ , and  $\text{Al}_6\text{C}_2$ ) usually have high ionization energies and open shell clusters ( $\text{Al}_3\text{C}_2$  and  $\text{Al}_5\text{C}_2$ ) usually have low ionization energies: for example,  $\text{Al}_3\text{C}_{2,4,\dots}$ , but not  $\text{Al}_3\text{C}_{1,3,\dots}$  clusters, and  $\text{Al}_5\text{C}_{1,3,\dots}$ , but not  $\text{Al}_5\text{C}_{2,4,\dots}$  clusters can be ionized by 6.4 eV photons. We investigate the HOMOs or SOMOs for a series of  $\text{Al}_m\text{C}_2$  ( $m = 2, 3, 4, 5, 6$ ) clusters, and find that the SOMOs for clusters  $\text{Al}_3\text{C}_2$ ,  $\text{Al}_3\text{C}_3$ , and  $\text{Al}_5\text{C}_2$ , (observed in 193 nm SPI experiments) possess an antibonding  $\pi$  molecular orbital character, while the HOMOs for clusters  $\text{Al}_2\text{C}_2$ ,  $\text{Al}_4\text{C}_2$ , and  $\text{Al}_6\text{C}_2$ , (not observed in 193 nm SPI experiments) are characterized by  $\sigma$  or  $\pi$  bonding molecular orbitals. These qualitative descriptions are based on both DFT canonical orbitals,<sup>17–21</sup> and DFT spin density plots for SOMOs. The VIEs thus obtained are qualitatively consistent with the orbital energies (HOMO or SOMOs) for the series. The calculational results are in good agreement with our experimental observations that  $\text{Al}_2\text{C}_2$ ,  $\text{Al}_2\text{C}_4$ , and  $\text{Al}_2\text{C}_6$  clusters cannot be detected through SPI by the 193 nm laser. Additionally,  $\text{Al}_3\text{C}_2$ ,  $\text{Al}_3\text{C}_3$ , and  $\text{Al}_5\text{C}_2$  are open shell molecules, but only  $\text{Al}_3\text{C}_2$  is detected by 6.4 eV SPI. The SOMOs for  $\text{Al}_5\text{C}_2$  and  $\text{Al}_3\text{C}_3$  clusters can be considered to be composed of a C=C antibonding  $\pi$  orbital and non bonding orbital (s and sp atomic orbitals) from Al atoms, while a pure C=C antibonding  $\pi$  orbital is the major component of the  $\text{Al}_3\text{C}_2$  cluster SOMO (see Fig. 9). Mixing between C=C antibonding  $\pi$  and Al non bonding orbitals apparently stabilizes the SOMO to some extent, leading to an increased of VIE. The HOMOs (SOMOs) of  $\text{Al}_2\text{C}_2\text{H}_x$  change from bonding orbitals ( $\text{Al}_2\text{C}_2$ ,  $\text{Al}_2\text{C}_2\text{H}_2$ ) to antibonding orbitals ( $\text{Al}_2\text{C}_2\text{H}$  and  $\text{Al}_2\text{C}_2\text{H}_3$ ) in agreement with our experimental observation of the ionization energy change of  $\text{Al}_2\text{C}_2\text{H}_x$  (see Fig. 11 and 12). HOMOs/SOMOs energy values of  $\text{Al}_m\text{C}_2$  clusters alternate as a function of the number of Al atoms in agreement with the experimental results and the VIE calculations.

## $\text{Al}_m\text{C}_n\text{H}_x$ clusters

$\text{Al}_m\text{C}_n\text{H}_x$  clusters can be generated by ablation of pure Al foil into a mixture of hydrocarbon/He expansion gas. Under this condition, aluminium metal vapor created by laser ablation reacts with hydrocarbon compounds in the ablation source, and then  $\text{Al}_m\text{C}_n\text{H}_x$  clusters are formed during a supersonic expansion and cooling processes. The distribution of the  $\text{Al}_m\text{C}_n\text{H}_x$  clusters detected by 193 nm laser ionization is presented in the mass spectra of Fig. 2. Only clusters with odd mass numbers are observed. Single photon energy of a 118 nm, 10.5 eV laser is sufficient to ionize most neutral metal compound clusters near threshold without leaving enough excess energy in the clusters to fragment the original neutral clusters.<sup>24</sup> If a 118 nm laser is used for ionization, all  $\text{Al}_m\text{C}_n\text{H}_x$  clusters with even and odd mass numbers are detected as shown in Fig. 5, indicating that all  $\text{Al}_m\text{C}_n\text{H}_x$  clusters are generated under the present experimental conditions. Therefore, some  $\text{Al}_m\text{C}_n\text{H}_x$  clusters must have higher ionization energies than the single photon energy of 193 nm light, resulting in the absence of these clusters in the 193 nm generated mass spectra. As we discussed above, the closed shell  $\text{Al}_m\text{C}_n$  clusters, such as  $\text{Al}_2\text{C}_m$ ,  $\text{Al}_4\text{C}_m$ , etc. have high ionization energies, and they cannot be ionized by 193 nm SPI (Fig. 1). The hydrogen containing clusters  $\text{Al}_2\text{C}_2\text{H}_{1,3,5,\dots}$ ,  $\text{Al}_2\text{C}_3\text{H}_{1,3,5,\dots}$ , and  $\text{Al}_4\text{C}_3\text{H}_{1,3,5,\dots}$ , with an odd number of H atoms are detected, while clusters  $\text{Al}_2\text{C}_2\text{H}_{2,4,6,\dots}$ ,  $\text{Al}_2\text{C}_3\text{H}_{2,4,6,\dots}$  and  $\text{Al}_4\text{C}_3\text{H}_{2,4,6,\dots}$ , with an even number of H atoms, are not detected by 193 nm SPI (Fig. 2–5). Adding an odd number of H atoms to closed shell  $\text{Al}_{2m}\text{C}_n$  clusters changes these clusters from closed shell to open shell electronic configurations, and thereby the ionization energies of these clusters can be below 6.4 eV. Open shell clusters  $\text{Al}_3\text{C}_{2,4,6,\dots}$  are detected by 193 nm SPI; however,  $\text{Al}_3\text{C}_2\text{H}_{1,3,5}$  and  $\text{Al}_3\text{C}_4\text{H}_{1,3,5}$  clusters with odd numbers of H atoms are not detected at this ionization energy, while  $\text{Al}_3\text{C}_2\text{H}_{2,4,6,\dots}$  and  $\text{Al}_3\text{C}_4\text{H}_{2,4,6,\dots}$  clusters are detected at this ionization energy. Adding an odd number of H atoms to the open shell clusters  $\text{Al}_3\text{C}_{2,4,6,\dots}$  changes their electronic structure from open shell to closed shell configurations, increasing the ionization energies of these clusters above 6.4 eV. Additionally, the open shell cluster  $\text{Al}_3\text{C}_3$  (VIE = 7.1 eV) is not detected by 6.4 eV SPI, but hydrogen containing open shell clusters  $\text{Al}_3\text{C}_3\text{H}_{2,4,8,\dots}$  are detected by 6.4 eV SPI (see Fig. 2–5): adding an even number of H atoms to these open shell clusters must change their electronic structures sufficiently to lower their VIEs below 6.4 eV. The exact value of a particular cluster VIE is thus a somewhat more subtle issue than simply open shell/closed shell electronic structures or single electron counting.

Signals are observed at mass numbers 89 and 116 amu (see Fig. 2, 3 and 5) that can be assigned to  $\text{Al}_2\text{C}_2\text{H}_{11}$  (89 amu) and  $\text{Al}_3\text{C}_2\text{H}_{11}$  (116 amu) clusters, respectively. Other possible products corresponding to mass number 89 amu, such as  $\text{AlC}_5\text{H}_2$  (89 amu),  $\text{AlC}_4\text{H}_{14}$  (89 amu) can be suggested; however, no  $\text{AlC}_5$  and  $\text{AlC}_4$  clusters are detected in the distribution of  $\text{Al}_m\text{C}_n$  clusters (see Fig. 1), and no  $\text{AlC}_5\text{H}_x$  and  $\text{AlC}_4\text{H}_x$  signals are identified in the isotope experiments (see Fig. 6). The  $\text{Al}_2\text{C}_2$  cluster (Fig. 1) and the  $\text{Al}_2\text{C}_2\text{H}_x$  clusters are, nonetheless, both identified (Fig. 6). Therefore,

we tentatively propose that the signal at 89 amu can be assigned to  $\text{Al}_2\text{C}_2\text{H}_{11}$ . Again, many possible products can be assigned to mass number 116 amu: for example,  $\text{Al}_2\text{C}_4\text{H}_{14}$  (116 amu) and  $\text{Al}_2\text{C}_5\text{H}_2$  (116 amu). The possibility of  $\text{Al}_2\text{C}_5\text{H}_2$  is very small since no  $\text{Al}_2\text{C}_5$  and  $\text{Al}_2\text{C}_5\text{H}_x$  are detected in either mass distribution.  $\text{Al}_2\text{C}_4\text{H}_{14}$  cluster is definitely a possible product corresponding to the signal at the mass number 116 amu because the  $\text{Al}_2\text{C}_4$  cluster is detected in  $\text{Al}_m\text{C}_n$  cluster experiments (Fig. 1) and  $\text{Al}_2\text{C}_4\text{H}_x$  clusters are identified in isotope experiments (Fig. 6). As shown in Fig. 6, the signal at mass number 105 amu consists of contributions from both  $\text{Al}_3\text{C}_2$  and  $\text{Al}_2\text{C}_4\text{H}_3$  clusters. Additionally,  $\text{Al}_2\text{C}_2\text{H}_{12}$  (90 amu) and  $\text{Al}_3\text{C}_2\text{H}_{12}$  (117 amu) clusters can not be uniquely distinguished because they overlap with other detected cluster signals,  $\text{Al}_2\text{C}_3$  (90 amu) and  $\text{Al}_3\text{C}_3$  (117 amu) (see Fig. 5), respectively. Here, we assume  $\text{Al}_2\text{C}_2\text{H}_{12}$  should also be generated in the ablation expansion source under the present experimental conditions.

Theoretical calculations are preformed to investigate the structures of  $\text{Al}_2\text{C}_2\text{H}_x$  clusters at the B3LYP/6-311+G\* theory level. As shown in Fig. 10, the hydrogen containing clusters  $\text{Al}_2\text{C}_2\text{H}_{1-4}$  are not saturated by H atoms, and the lowest energy isomer structures for these clusters are similar to those for unsaturated hydrocarbons. In these structures, H atoms bond to either C or Al atoms with little difference in energy. This fact can account for the general richness of different structures for these  $\text{Al}_m\text{C}_n\text{H}_x$  clusters. Clusters  $\text{Al}_2\text{C}_2\text{H}_8$  have a saturated structure, like hydrocarbons  $\text{C}_n\text{H}_{2n+2}$ , for hydrogen containing  $\text{Al}_m\text{C}_n\text{H}_x$  clusters with classical Al–H and C–H bonds.

Experiments show that clusters containing more than 8 hydrogen atoms, such as  $\text{Al}_2\text{C}_2\text{H}_{9-11}$  (193 nm ionization experiment, Fig. 2 and 3) and  $\text{Al}_2\text{C}_2\text{H}_{9-12}$  (118 nm ionization experiment, Fig. 5) are readily identified in the mass spectra, indicating that hydrogen containing clusters  $\text{Al}_2\text{C}_2\text{H}_{9-12}$  are generated under the present experimental condition. We do not find a stable structure for  $\text{Al}_2\text{C}_2\text{H}_{12}$  that is built on saturated, classical Al–H and C–H chemical bonds; however,  $\text{H}_2$  molecules can possibly be adsorbed on  $\text{Al}_m\text{C}_n/\text{Al}_m\text{C}_n\text{H}_x$  clusters through chemisorption, causing more hydrogen to be associated with the clusters than can be accounted for by a saturated classical chemical bond structure. Recently, Durgun *et al.*<sup>35–37</sup> calculated  $\text{H}_2$  adsorption on a transition metal-ethylene  $\text{C}_2\text{H}_4\text{M}_2$  (TM-ethylene) complex, in which two metal atoms are bonded to a C=C moiety through a bridge structure. They find that, based on calculations, up to 12  $\text{H}_2$  molecules can be adsorbed around the  $\text{C}_2\text{H}_4\text{Ti}_2$  complex: up to ~14 wt% hydrogen storage for this complex. We can not positively identify  $\text{Al}_m\text{C}_n\text{H}_x$  clusters containing more than 12 H atoms in the mass spectra, since the mass number of carbon is 12.

To understand the effect of H atoms on the ionization energies of aluminium carbon hydride clusters, we perform *ab initio* calculations to study the VIEs of  $\text{Al}_m\text{C}_n\text{H}_x$  species at the MP2/6-311+G\* theory level. As plotted in Fig. 11, the VIEs of  $\text{Al}_2\text{C}_2\text{H}_x$  clusters change with the number of H atoms. The alternation tends of calculated VIEs of the  $\text{Al}_m\text{C}_n$  and  $\text{Al}_m\text{C}_n\text{H}_x$  clusters are in good agreement with our experimental observations that systematically some members of the

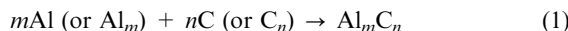
$\text{Al}_m\text{C}_n$  and  $\text{Al}_m\text{C}_n\text{H}_x$  cluster distributions have low VIEs and some have high VIEs. This observed VIE alternation depends on the numbers of Al, C, and H atoms in the clusters and the calculations completely explain the experimental observations. Therefore, we believe that the predicted structures of the calculated clusters are correct due to the specific and systematic agreement of theory and experiment.

The highest occupied orbitals for a selection of  $\text{Al}_2\text{C}_2\text{H}_x$  clusters are calculated at the B3LYP/6-311+G\* level, and shown in Fig. 12. SOMOs for open shell clusters  $\text{Al}_2\text{C}_2\text{H}$  and  $\text{Al}_2\text{C}_2\text{H}_3$  are antibonding  $\pi$  orbitals characteristic of a C=C moiety. HOMOs for the closed shell clusters  $\text{Al}_2\text{C}_2$ ,  $\text{Al}_2\text{C}_2\text{H}_2$ , and  $\text{Al}_2\text{C}_2\text{H}_4$  are characterized as either bonding  $\sigma$  and non bonding orbitals of the Al atom, or bonding  $\pi$  orbitals of the C=C atoms. The number of H atoms in the clusters switches the  $\text{Al}_2\text{C}_2\text{H}_x$  between closed shell and open shell systems, leading to VIE alternation with even-odd numbers of H atoms in the clusters. Additionally, the open shell  $\text{Al}_3\text{C}_2$  cluster (VIE = 6.4 eV) is detected by SPI at 193 nm due to its relatively low VIE; adding one H to the  $\text{Al}_3\text{C}_2$  cluster yields a closed shell cluster ( $\text{Al}_3\text{C}_2\text{H}$ ) with VIE about 7.5 eV, and adding two H atoms to  $\text{Al}_3\text{C}_2$  yields  $\text{Al}_3\text{C}_2\text{H}_2$  with a VIE of 6.9 eV. The HOMOs/SOMOs of  $\text{Al}_3\text{C}_2\text{H}_{0,1,2}$  change with the number of H atoms as shown in Fig. 9 and 12. HOMOs/SOMOs energy values of  $\text{Al}_2\text{C}_2\text{H}_x$  clusters also alternate as a function of the number of H atoms in agreement with the experimental results and the VIE calculations. The calculational results for the HOMO/SOMO characteristics and patterns of the  $\text{Al}_m\text{C}_n\text{H}_x$  clusters give us a qualitative understanding of the experimental observations.

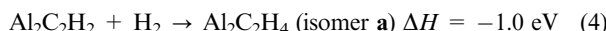
### Synthetic reaction mechanisms for $\text{Al}_m\text{C}_n$ and $\text{Al}_m\text{C}_n\text{H}_x$

The mechanism for  $\text{Al}_m\text{C}_n\text{H}_x$  cluster formation is very complicated in the ablation/expansion source. As discussed in the Experimental section, by using method (1), Al atoms and clusters generated from ablation of Al metal can react with hydrocarbons in the expansion gas to form  $\text{Al}_m\text{C}_n\text{H}_x$  clusters in the ablation/expansion source. This hydrocarbon plasma reaction synthetic method is also the most efficient route for generation of pure metal carbide clusters for reactive early transition metals (Ti, V, Zr, Nb, Hf, Cr, Mo, Fe),<sup>1–3,38</sup> but the method cannot be used to generate pure metal carbide clusters for less reactive, later transition metals or main group metals (Ni, Co, W, Ag, Cu, Bi, Sb).<sup>39</sup> A mechanism can be suggested for  $\text{M}_m\text{C}_n$  cluster generation: the ablated  $\text{M}_m$  species and ensuing plasma can interact with (and heat)  $\text{C}_x\text{H}_y$  molecules to form  $\text{C}_z$  and H species which can react with  $\text{M}_m$  clusters ( $m \geq 1$ ) in the plasma. Metal carbide clusters  $\text{M}_m\text{C}_n$  are formed by the reaction of metal and carbon atoms/carbon clusters during the expansion and cooling processes.<sup>38</sup> Al atoms and clusters are thus a unique set of species with regard to reactions with hydrocarbons. Five different experiments have been performed in these studies to try to discover the nature of the reactions that generate  $\text{Al}_m\text{C}_n\text{H}_x$  species: 1. ablation of Al metal into expansion gas containing hydrocarbons, yielding  $\text{Al}_m\text{C}_n\text{H}_x$ ; 2. ablation of Al metal into pure hydrogen, yielding almost  $\text{Al}_m$  only. 3. ablation of an Al/C pellet into He, yielding  $\text{Al}_m\text{C}_n$ ; 4. ablation of an Al/C

pellet into H<sub>2</sub> gas, yielding Al<sub>*m*</sub>C<sub>*n*</sub>H<sub>*x*</sub>; and 5. ablation of an Al/C pellet into He and passage of cooled Al<sub>*m*</sub>C<sub>*n*</sub> species into a fast flow tube reactor containing H<sub>2</sub>, yielding Al<sub>*m*</sub>C<sub>*n*</sub>H<sub>*x*</sub> clusters. This combination of experiments makes it clear that the reaction process to generate Al<sub>*m*</sub>C<sub>*n*</sub> and Al<sub>*m*</sub>C<sub>*n*</sub>H<sub>*x*</sub> species is as follows:



On the basis of our calculations, hydrogenation reactions for Al<sub>2</sub>C<sub>2</sub> and H<sub>2</sub> molecules are thermodynamically favorable. For example,



Therefore, Al<sub>*m*</sub>C<sub>*n*</sub>H<sub>*x*</sub> clusters can be generated by reactions between Al<sub>*m*</sub>C<sub>*n*</sub> clusters and H<sub>2</sub> molecules. Al<sub>*m*</sub>C<sub>*n*</sub> clusters react with H<sub>2</sub> in the fast flow reactor (at *ca.* 300–400 K), and Al<sub>*m*</sub>C<sub>*n*</sub>H<sub>*x*</sub> clusters containing even and odd numbers of H atoms are generated through these reactions. Based on our calculations, reactions Al<sub>*m*</sub>C<sub>*n*</sub> + yH<sub>2</sub> are exothermic, so that H<sub>2</sub> can be dissociated on Al<sub>*m*</sub>C<sub>*n*</sub> clusters to form Al<sub>*m*</sub>C<sub>*n*</sub>H<sub>*x*</sub> clusters, *x* = 1, 2, . . . , 12. Note that the most stable structures for small Al<sub>*m*</sub>C<sub>*n*</sub> clusters have linear geometries with unsaturated C–C bonds and not cubic frame structures (Fig. 7) based on our calculational results. These linear, multiple C–C bonded structures enable Al<sub>*m*</sub>C<sub>*n*</sub> cluster reactions with hydrogens to form Al<sub>*m*</sub>C<sub>*n*</sub>H<sub>*x*</sub> clusters.

Based on the present studies, Al<sub>*m*</sub>C<sub>*n*</sub>H<sub>*x*</sub> clusters can be a potential material for hydrogen storage. Hydrogen is an ideal clean fuel for storage, transport, and conversion of energy. A design target for automobile fueling has been set by the U. S. Department of Energy at 6.5% hydrogen by weight. Recently, intensive research has been initiated on complex aluminium hydrides M<sub>*m*</sub>Al<sub>*n*</sub>H<sub>*x*</sub> (M = Li, Na, Mg, B, Ti, Zr) for hydrogen storage, as these compounds have high hydrogen storage capacity (10.54% wt H for LiAlH<sub>4</sub>, 7.41% wt H for NaAlH<sub>4</sub>), low cost, and bulk availability.<sup>24,40–46</sup> Al<sub>*m*</sub>C<sub>*n*</sub>H<sub>*x*</sub> clusters also have a high percentage of hydrogen by weight: for example, 13.3 wt% H for an Al<sub>2</sub>C<sub>2</sub>H<sub>12</sub> cluster, 10.25 wt% H for an Al<sub>3</sub>C<sub>2</sub>H<sub>12</sub> cluster, and 12.8 wt% H for an Al<sub>2</sub>C<sub>4</sub>H<sub>15</sub> cluster. Here we assume that Al<sub>2</sub>C<sub>2</sub>H<sub>12</sub>, Al<sub>3</sub>C<sub>2</sub>H<sub>12</sub>, or Al<sub>2</sub>C<sub>4</sub>H<sub>15</sub> could be generated in the ablation expansion source under our experimental conditions, as we discuss above. Additionally, H atoms can bond with either Al or C atoms in these clusters with little energy difference for the various possible cluster isomers. Hydrocarbons have high hydrogen content, but they are not good materials for hydrogen fuel storage since high energy is required to release H<sub>2</sub> from them due to their C–H bond strength (104 kcal mol<sup>-1</sup> for CH<sub>4</sub>, and 125 kcal mol<sup>-1</sup> for C<sub>2</sub>H<sub>4</sub>). The Al–H bond strength (68 kcal mol<sup>-1</sup>)<sup>47</sup> is much weaker than the C–H bond strength and thus less energy is required for dehydrogenation of Al<sub>*m*</sub>C<sub>*n*</sub>H<sub>*x*</sub> clusters than for C<sub>*x*</sub>H<sub>*y*</sub> molecules. Additionally, through the reaction Al<sub>*m*</sub> + C<sub>*x*</sub>H<sub>*y*</sub> → Al<sub>*m*</sub>C<sub>*n*</sub>H<sub>*y*</sub> → y/2 H<sub>2</sub> + Al<sub>*m*</sub>C<sub>*n*</sub>, hydrogen fuel is non polluting compared to a hydrocarbons fuel.

## Conclusions

Neutral Al<sub>*m*</sub>C<sub>*n*</sub> and Al<sub>*m*</sub>C<sub>*n*</sub>H<sub>*x*</sub> clusters are observed and systematically studied for the first time by experimental and theoretical methods. Only some of the neutral Al<sub>*m*</sub>C<sub>*n*</sub> and Al<sub>*m*</sub>C<sub>*n*</sub>H<sub>*x*</sub> clusters with odd mass numbers (*i.e.*, an odd number of electrons) have low VIEs. Systematic variation of the VIEs of Al<sub>*m*</sub>C<sub>*n*</sub> and Al<sub>*m*</sub>C<sub>*n*</sub>H<sub>*x*</sub> clusters with the numbers of Al, C and H atoms is observed. Based on our calculations, the VIEs of Al<sub>*m*</sub>C<sub>*2*</sub> (*m* = 2, 3, 4, 5, 6) clusters change with odd–even numbers of Al atoms because the electronic structures of the clusters change from open shell to closed shell configurations, respectively. VIEs of neutral Al<sub>2</sub>C<sub>2</sub>H<sub>*x*</sub> (*x* = 0, 1, 2, 3, 4) clusters change with the number of H atoms, because adding H atoms to the clusters changes the electronic configuration of the clusters from open shell to closed shell and *vice versa*. Theory and experiment agree on this major observation, indicating that predicted geometrical and electronic structures for the calculated Al<sub>*m*</sub>C<sub>*n*</sub> and Al<sub>*m*</sub>C<sub>*n*</sub>H<sub>*x*</sub> clusters are most likely correct. Based on calculations, HOMOs for the closed shell clusters Al<sub>2*n*</sub>C<sub>2</sub> (Al<sub>2</sub>C<sub>2</sub>, Al<sub>4</sub>C<sub>2</sub>, and Al<sub>6</sub>C<sub>2</sub>) and Al<sub>2</sub>C<sub>2</sub>H<sub>*n*</sub> (Al<sub>2</sub>C<sub>2</sub>H<sub>2</sub> and Al<sub>2</sub>C<sub>2</sub>H<sub>4</sub>) can be generally characterized as bonding  $\pi$  or  $\sigma$  orbitals, and SOMOs for the open shell clusters Al<sub>2*m*+1</sub>C<sub>*n*</sub> (Al<sub>3</sub>C<sub>2</sub>, Al<sub>3</sub>C<sub>3</sub>, and Al<sub>5</sub>C<sub>2</sub>) and Al<sub>2</sub>C<sub>2</sub>H<sub>*n*+1</sub> (Al<sub>2</sub>C<sub>2</sub>H and Al<sub>2</sub>C<sub>2</sub>H<sub>3</sub>) can be generally characterized as antibonding  $\pi$  orbitals.

A large number of Al<sub>*m*</sub>C<sub>*n*</sub>H<sub>*x*</sub> clusters (but not pure Al<sub>*m*</sub>C<sub>*n*</sub>) are generated by a hydrocarbon plasma synthesis reaction method, while only pure metal carbide M<sub>*m*</sub>C<sub>*n*</sub> clusters are generated for most transition metals under the same synthesis conditions. Moreover, Al<sub>*m*</sub>C<sub>*n*</sub>H<sub>*x*</sub> clusters can also be generated from the reaction of Al<sub>*m*</sub>C<sub>*n*</sub> + yH<sub>2</sub> at low temperature in a fast flow reactor. These observations imply that the formation mechanism, Al<sub>*m*</sub> (*m* = 1, 2, . . .) + C<sub>*n*</sub> (*n* = 1, 2, . . .) + yH<sub>2</sub> → Al<sub>*m*</sub>C<sub>*n*</sub> + yH<sub>2</sub> → Al<sub>*m*</sub>C<sub>*n*</sub>H<sub>*x*</sub>, can be postulated. The structures of Al<sub>*m*</sub>C<sub>*n*</sub> clusters and their chemistry must thereby be different from those of most transition metal carbide clusters. On the basis of the calculational results, the structures with C=C bonds are energetically favorable for small neutral Al<sub>*m*</sub>C<sub>*n*</sub> clusters. All calculated low energy cluster structures have singlet or doublet spin multiplicities. Al<sub>*m*</sub>C<sub>*n*</sub>H<sub>*x*</sub> clusters have unique properties that make them a potential hydrogen storage material; for example, up to 13% hydrogen storage by weight can be achieved for Al<sub>2</sub>C<sub>2</sub>H<sub>12</sub>.

## Acknowledgements

We have had many fruitful discussions with Prof. A. K. Rappe concerning calculation of the molecular orbitals for the clusters discussed in this report. This work is supported by AFOSR, the NSF ERC for Extreme Ultraviolet Science and Technology under NSF Award No. 0310717, and the National Center for Supercomputing Applications under grant CHE090039.

## References

- (a) B. C. Guo, K. P. Kerns and A. W. Castleman, Jr., *Science*, 1992, **255**, 1411; (b) B. C. Guo, S. Wei, J. Purnell, S. Buzzia and A. W. Castleman, Jr., *Science*, 1992, **256**, 515; (c) S. Wei,

- B. C. Guo, J. Purnell, S. Buzz and A. W. Castleman, Jr., *Science*, 1992, **256**, 818.
- 2 (a) M. M. Rohmer, M. Benard and J. M. Poblet, *Chem. Rev.*, 2000, **100**, 495; (b) D. van Heijnsbergen, G. von Helden, M. A. Duncan, A. J. A. van Roij and G. Meijer, *Phys. Rev. Lett.*, 1999, **83**, 4983; (c) M. A. Duncan, *J. Cluster Sci.*, 1997, **8**, 239.
- 3 (a) S. F. Cartier, B. D. May and A. W. Castleman, Jr., *J. Am. Chem. Soc.*, 1994, **116**, 5295; (b) S. F. Cartier, B. D. May and A. W. Castleman, Jr., *J. Chem. Phys.*, 1994, **100**, 5384; (c) S. Wei, B. C. Guo, H. T. Deng, K. Kerns, J. Purnell, S. Buzz and A. W. Castleman, Jr., *J. Am. Chem. Soc.*, 1994, **116**, 4475–4476; (d) J. S. Pilgrim and M. A. Duncan, *J. Am. Chem. Soc.*, 1993, **115**, 9724; (e) C. S. Yeh, Y. G. Byun, S. Afzaal, S. Z. Kan, S. Lee, B. S. Freiser and P. J. Hay, *J. Am. Chem. Soc.*, 1995, **117**, 4042–4048; (f) J. S. Pilgrim and M. A. Duncan, *J. Am. Chem. Soc.*, 1993, **115**, 6958–6961; (g) S. Li, H. Wu and L. S. Wang, *J. Am. Chem. Soc.*, 1997, **119**, 7417–7422.
- 4 (a) K. Tono, A. Terasaki, T. Ohta and T. Kondow, *J. Chem. Phys.*, 2002, **117**, 7010; (b) Y. Yamada and A. W. Castleman, Jr., *Chem. Phys. Lett.*, 1993, **204**, 133–138.
- 5 J. S. Pilgrim and M. A. Duncan, *J. Am. Chem. Soc.*, 1993, **115**, 4395.
- 6 A. I. Boldyrev and J. Simons, *J. Phys. Chem. A*, 1997, **101**, 2215.
- 7 K. L. Knappenberger, Jr., C. E. Jones, Jr., M. A. Sobny, I. Iordanov, J. Sofo and A. W. Castleman, Jr., *J. Phys. Chem. A*, 2006, **110**, 12814.
- 8 W. Pan and W. T. Yang, *Phys. Rev. B: Condens. Matter*, 1995, **51**, 3610.
- 9 S. G. He, Y. Xie, F. Dong and E. R. Bernstein, *J. Chem. Phys.*, 2006, **125**, 164306.
- 10 L. R. Brock and M. A. Duncan, *J. Phys. Chem.*, 1996, **100**, 5654.
- 11 G. V. Gueorguiev and J. M. Pacheco, *Phys. Rev. B*, 2003, **68**, 241401(R).
- 12 M. W. Heaven, G. M. Stewart, M. A. Buntine and G. F. Metha, *J. Phys. Chem. A*, 2000, **104**, 3308.
- 13 (a) V. Dryza, M. A. Addicoat, J. R. Gascooke, M. A. Buntine and G. F. Metha, *J. Phys. Chem. A*, 2008, **112**, 5582; (b) V. Dryza, M. A. Addicoat, J. R. Gascooke, M. A. Buntine and G. F. Metha, *J. Phys. Chem. A*, 2005, **109**, 11180.
- 14 L. S. Wang and H. S. Cheng, *Phys. Rev. Lett.*, 1997, **78**, 2983.
- 15 L. S. Wang, X. B. Wang, H. B. Wu and H. Cheng, *J. Am. Chem. Soc.*, 1998, **120**, 6556.
- 16 B. W. Ticknor, B. Bandyopadhyay and M. A. Duncan, *J. Phys. Chem. A*, 2008, **112**, 12355.
- 17 A. I. Boldyrev, J. Simons, X. Li and L. S. Wang, *J. Am. Chem. Soc.*, 1999, **121**, 10193.
- 18 X. Li, L. S. Wang, W. Chen, A. I. Boldyrev and J. Simons, *J. Am. Chem. Soc.*, 1999, **121**, 6033.
- 19 (a) N. Cannon, A. I. Boldyrev, X. Li and L. S. J. Wang, *J. Chem. Phys.*, 2000, **113**, 2671; (b) X. Li, L. S. Wang, N. Cannon and A. I. Boldyrev, *J. Chem. Phys.*, 2002, **116**, 1330.
- 20 X. Li, H. F. Zhang, L. S. Wang, G. D. Geske and A. I. Boldyrev, *Angew. Chem., Int. Ed.*, 2000, **39**, 3630.
- 21 (a) A. I. Boldyrev, J. Simons, X. Li and L. S. Wang, *J. Chem. Phys.*, 1999, **111**, 4993; (b) A. I. Boldyrev, J. Simons, X. Li, W. Chen and L. S. Wang, *J. Chem. Phys.*, 1999, **110**, 8980; (c) D. Y. Zubarev and A. I. Boldyrev, *J. Chem. Phys.*, 2005, **122**, 144322.
- 22 F. Y. Naumkin, *J. Phys. Chem. A*, 2008, **112**, 4660.
- 23 (a) J. C. Zhao, D. A. Knight, G. M. Brown, C. Kim, Son-Jong Hwang, J. W. Reiter, R. C. Bowman, Jr., J. A. Zan and J. G. Kulleck, *J. Phys. Chem. C*, 2009, **113**, 2; (b) A. Zuttel, *Naturwissenschaften*, 2004, **91**, 157.
- 24 (a) F. Dong, S. Heinbuch, Y. Xie, E. R. Bernstein, J. J. Rocca, Z. C. Wang, X. L. Ding and S. G. He, *J. Am. Chem. Soc.*, 2009, **131**, 1507; (b) F. Dong, S. Heinbuch, Y. Xie, J. J. Rocca, E. R. Bernstein, Z. C. Wang, K. Deng and S. G. He, *J. Am. Chem. Soc.*, 2008, **130**, 1932; (c) F. Dong, S. Heinbuch, J. J. Rocca and E. R. Bernstein, *J. Chem. Phys.*, 2006, **125**, 164318.
- 25 (a) S. Heinbuch, M. Grisham, D. Martz and J. J. Rocca, *Opt. Express*, 2005, **13**, 4050; (b) J. J. Rocca, V. N. Shlyaptev, F. G. Tomasel, O. D. Cortazar, D. Hartshorn and J. L. A. Chilla, *Phys. Rev. Lett.*, 1994, **73**, 2192; (c) J. J. Rocca, *Rev. Sci. Instrum.*, 1999, **70**, 3799.
- 26 L. Belau, K. R. Wilson, S. R. Leone and M. Ahmed, *J. Phys. Chem. A*, 2007, **111**, 10075.
- 27 M. J. Frisch, G. W. Trucks, H. B. Schlegel, G. E. Scuseria, M. A. Robb, J. R. Cheeseman, J. A. Montgomery, Jr., T. Vreven, K. N. Kudin, J. C. Burant, J. M. Millam, S. S. Iyengar, J. Tomasi, V. Barone, M. Mennucci, M. Cossi, G. Scalmani, N. Rega, G. A. Petersson, H. Nakatsuji, M. Hada, M. Ehara, K. Toyota, R. Fukuda, J. Hasegawa, M. Ishida, T. Nakajima, Y. Honda, O. Kitao, H. Nakai, M. Klene, X. Li, J. E. Knox, H. P. Hratchian, J. B. Cross, V. Bakken, C. Adamo, J. Jaramillo, R. Gomperts, R. E. Stratmann, O. Yazyev, A. J. Austin, R. Cammi, C. Pomelli, J. W. Ochterski, P. Y. Ayala, K. Morokuma, G. A. Voth, P. Salvador, J. J. Dannenberg, V. G. Zakrzewski, S. Dapprich, A. D. Daniels, M. C. Strain, O. Farkas, D. K. Malick, A. D. Rabuck, K. Raghavachari, J. B. Foresman, J. V. Ortiz, Q. Cui, A. G. Baboul, S. Clifford, J. Cioslowski, B. B. Stefanov, G. Liu, A. Liashenko, P. Piskorz, I. Komaromi, R. L. Martin, D. J. Fox, T. Keith, M. A. Al-Laham, C. Y. Peng, A. Nanayakkara, M. Challacombe, P. M. W. Gill, B. Johnson, W. Chen, M. W. Wong, C. Gonzalez and J. A. Pople, *GAUSSIAN 03, Revision C.02*, Gaussian, Inc., Wallingford, CT, 2004.
- 28 (a) A. D. Becke, *Phys. Rev. A: At., Mol., Opt. Phys.*, 1988, **38**, 3098; (b) A. D. Becke, *J. Chem. Phys.*, 1993, **98**, 5648; (c) C. T. Lee, W. T. Yang and R. G. Parr, *Phys. Rev. B: Condens. Matter*, 1988, **37**, 785.
- 29 (a) A. D. McLean and G. S. Chandler, *J. Chem. Phys.*, 1980, **72**, 5639; (b) T. Clark, J. Chandrasekhar, G. W. Spitznagel and P. V. R. Schleyer, *J. Comput. Chem.*, 1983, **4**, 294; (c) M. J. Frisch, J. A. Pople and J. S. Binkley, *J. Chem. Phys.*, 1984, **80**, 3265.
- 30 R. Krishnan, J. S. Binkley, R. Seeger and J. A. Pople, *J. Chem. Phys.*, 1980, **72**, 650.
- 31 A. Largo, P. Redondo and C. Barrientos, *J. Phys. Chem. A*, 2002, **106**, 4217.
- 32 G. L. Li and Z. Tang, *J. Phys. Chem. A*, 2003, **107**, 5317.
- 33 (a) F. Dong, S. Heinbuch, J. J. Rocca and E. R. Bernstein, *J. Chem. Phys.*, 2006, **124**, 224319; (b) F. Dong, S. Heinbuch, J. J. Rocca and E. R. Bernstein, *J. Chem. Phys.*, 2006, **125**, 154317; (c) S. Heinbuch, F. Dong, J. J. Rocca and E. R. Bernstein, *J. Chem. Phys.*, 2006, **125**, 154316; (d) S. Heinbuch, F. Dong, J. J. Rocca and E. R. Bernstein, *J. Chem. Phys.*, 2007, **126**, 244301.
- 34 C. W. Robert and J. A. Melvin, *CRC hand book of chemistry and Physics 62nd*, CRC Press, Inc., 1981–1982.
- 35 E. Durgun, S. Ciraci, W. Zhou and T. Yildirim, *Phys. Rev. Lett.*, 2006, **97**, 226102.
- 36 W. Zhou, T. Yildirim, E. Durgun and S. Ciraci, *Phys. Rev. B*, 2007, **76**, 085434.
- 37 N. Akman, E. Durgun, T. Yildirim and S. Ciraci, *J. Phys.: Condens. Matter*, 2006, **18**, 9509.
- 38 B. C. Guo, S. Wei, Z. Chen, K. P. Kerns, J. Purnell, S. Buzz and A. W. Castleman, Jr., *J. Chem. Phys.*, 1992, **97**, 5243.
- 39 J. E. Reddic and M. A. Duncan, *Chem. Phys. Lett.*, 1997, **264**, 157.
- 40 X. Li, A. Grubisic, S. T. Stoker, J. Cordes, G. F. Gantefor, K. H. Bowen, B. Kiran, M. Willis, P. Jena, R. Burgert and H. Schnockel, *Science*, 2007, **315**, 356.
- 41 A. Grubisic, X. Li, S. T. Stoker, J. Cordes, G. F. Gantefor, K. H. Bowen, B. Kiran, P. Jena, R. Burgert and H. Schnockel, *J. Am. Chem. Soc.*, 2007, **129**, 5969.
- 42 M. Felderhoff, C. Weidenthaler, R. von Helmolt and U. Rberle, *Phys. Chem. Chem. Phys.*, 2007, **9**, 2643.
- 43 S. Orimo, N. Nakamori, J. R. Rliseo, A. Zuttel and C. M. Jensen, *Chem. Rev.*, 2007, **107**, 4111.
- 44 B. Sakintuna, F. Lamari-Darkrim and M. Hirscher, *Internal J. Hydrogen Energy*, 2007, **32**, 1121.
- 45 M. Fichtner, J. Engel, O. Fuhr, O. Kircher and O. Rubner, *Materials Science and Engineering B*, 2004, **108**, 42.
- 46 A. W. C. van den Berg and C. O. Arean, *Chem. Commun.*, 2008, 668.
- 47 M. W. Chase, Jr. NIST-JANAF Thermochemical Tables, *J. Phys. Chem. Ref. Data*, Monograph 9, Fourth Edition, 1998, pp. 1–1951.